Vitamin D constrains inflammation by modulating the expression of key genes on Chr17q12-21.1

Ayşe Kılıç[1*], Arda Halu[1], Margherita De Marzio[1,2], Enrico Maiorino[1], Melody G. Duvall[3], Thayse Brueggemann[3], Joselyn J. Rojas Quintero[3], Robert Chase[1], Hooman Mirzakhani[1], Ayse Özge Sungur[4, 5], Janine Koepke[5], Taiji Nakano[6], Hong Yong Peh[3], Nandini Krishnamoorthy[3], Raja-Elie Abdulnour[3], Katia Georgopoulos[7], Augusto A. Litonjua[8], Marie B. Demay[9], Harald Renz[10, 11], Bruce D. Levy[3] and Scott. T Weiss[1*]

Affiliations:

1. Channing Division of Network Medicine, Department of Medicine, Brigham and Women's Hospital and Harvard Medical School, Boston MA, USA
2. Department of Environmental Health, Harvard TH Chan School of Public Health, Boston, MA, USA
3. Division of Pulmonary and Critical Care Medicine, Department of Medicine, Brigham and Women's Hospital and Harvard Medical School, Boston, MA, USA.
4. Behavioral Neuroscience, Experimental and Biological Psychology, Philipps-University Marburg, Marburg, Germany
5. Excellence Cluster Cardio-Pulmonary System (ECCPS), Justus Liebig University Giessen, Giessen, Germany
6. Department of Pediatrics, Graduate School of Medicine, Chiba University, Chiba, Japan
7. Cutaneous Biology Research Center, Massachusetts General Hospital, Harvard Medical School, Charlestown, Massachusetts, USA

8. Division of Pediatric Pulmonary Medicine, Golisano Children's Hospital at Strong, University of Rochester Medical Center, Rochester, NY, USA
9. Endocrine Unit, Massachusetts General Hospital and Harvard Medical School, Boston, MA, USA
10. Institute of Laboratory Medicine and Pathobiochemistry, Molecular Diagnostics, Philipps University of Marburg, Marburg, Germany; German Center for Lung Research (DZL).
11. Department of Clinical Immunology and Allergology, Laboratory of Immunopathology, Sechenov University, Moscow, Russia

*Correspondence should be addressed to A.K. (ayskilic@gmail.com) or S.T.W (scott.weiss@channing.harvard.edu).

Keywords: Vitamin D, airway inflammation, Th2 cells, Chr17q12-21, autoimmunity, immunomodulation, AIOLOS

Summary

Vitamin D possesses immunomodulatory functions and vitamin D deficiency has been associated with the rise in chronic inflammatory diseases, including asthma [1]. Vitamin D supplementation studies do not provide insight into the molecular genetic mechanisms of vitamin D mediated immunoregulation. Here we provide evidence for vitamin D regulation of two human chromosomal loci, Chr17q12-21.1 and Chr17q21.2, reliably associated with autoimmune and chronic inflammatory diseases [2–4]. We demonstrate increased vitamin D receptor (VDR) expression in mouse lung CD4+ Th2 cells, differential expression of Chr17q12-21.1 and Chr17q21.2 genes in Th2 cells based on vitamin D status and identify the IL-2/Stat5 pathway as a target of vitamin D signaling. Vitamin D deficiency caused

52 severe lung inflammation after allergen challenge in mice that was prevented by long term
53 prenatal vitamin D supplementation. Mechanistically, vitamin D induced the expression
54 of the *Ikzf3* encoded protein Aiolos to suppress IL-2- signaling and ameliorate cytokine
55 production in Th2 cells. These translational findings demonstrate mechanisms for the
56 immune protective effect of vitamin D in allergic lung inflammation with a strong molecular
57 genetic link to the regulation of both Chr17q12-21.1 and Chr17q21.2 genes and suggest
58 further functional studies and interventional strategies for long- term prevention of asthma
59 and other autoimmune disorders.
60
61 **Results**
62
63 To address the genetic and molecular mechanisms by which vitamin D can influence
64 asthma, allergic and autoimmune disease risk, we studied the genetic loci of two
65 chromosome regions of interest: 1) the 17q12-21.1 region, that includes the well-known
66 asthma-associated *ORMDL3* gene [5], and 2) the 17q21.2 region, that includes the *STAT5*
67 gene, known to be extensively associated with autoimmune diseases [6,7]. We first
68 examined the entire set of significant disease and trait associations in the Chr17q12-21.1
69 (181 associations) and Chr17q21.2 (100 associations) loci using the NHGRI-EBI GWAS
70 Catalog [8]. Both regions had multiple Th1 and Th2 diseases associations with at least one
71 significant SNP. Chr17q12-21.1 had the highest number of associations related to Th2
72 diseases (Fig. 1a) and 17q21.2 had the highest number of associations related to Th1
73 diseases (Extended Data Fig. 1a). To address the possible link to vitamin D intake, we
74 next investigated a potential overlap of these SNPs with VDR binding sites. Out of the
75 169 VDR binding sites on Chr17, seven were located in the 17q12-21.1 locus,
76 concentrated in two bands on or near *IKZF3* and *ZPBP2* (Fig. 1b). These VDR binding
77 sites also overlapped with RXRA binding sites (Fig. 1b). To assess their functional
78 relevance, we searched for eQTLs in these VDR binding regions. We found that four cis-
79 eQTLs control *IKZF3* expression in whole blood and EBV-transformed lymphocytes:
80 rs2941522 and rs12946510 in the enhancer region targeting *ORMDL3* and *IKZF3*, and
81 rs1453559 and rs35564481 in the enhancer region targeting *ORMDL3*, *GSDMA* and
82 *GSDMB* (Fig. 1b). Rs1453559 and rs2941522 have previous GWAS associations with

both asthma and autoimmune diseases[9–11], rs12946510 has previous GWAS associations with autoimmune diseases[12,13], and rs35564481 has no known GWAS associations. For the 17q21.2 locus, the only VDR binding site resides near the gene *PSMC3IP* in an enhancer site targeting *STAT5A* (Extended Data. Fig. 1b). PSMC3IP expression is controlled by three eQTLs overlapping with this VDR binding site (rs4793244, rs62078362 and rs111708606), none of which have any known disease associations. These results suggest that vitamin D binding is critical in this genomic region.

We next examined the linkage disequilibrium (LD) pattern between the Th1/Th2-associated SNPs and the SNPs in the VDR binding sites (Fig. 1c). Out of the seven SNPs with VDR binding sites identified in 17q12-21.1 and 17q21.2, the first four in 17q12-21.1 (rs2941522, rs12946510, rs35564481, rs1453559) were in a high-LD block with many other Th1-Th2 associated SNPs in the same region. These same four SNPs in 17q12-21.1 were also in high-LD with two SNPs in *ZPBP2* and *ORMDL3* (rs12936231 and rs4065275, respectively) that were previously shown to be functionally relevant to asthma [3,4,14]. Additionally, two of the three SNPs with VDR binding sites in 17q21.2 (rs4793244 and rs62078362) were in strong-LD with three other Th1-Th2 associated SNPs in the17q21.2 region (rs11871801, rs2006141, rs4793090). Overall, these results highlight strong statistical association between vitamin D binding sites and multiple genotypic variations linked to asthma, autoimmune and allergic diseases.

Two SNPs in *ZPBP2* and *ORMDL3* (rs12936231 and rs4065275, respectively) that were previously shown to be functionally relevant to asthma [3,4,14], were also in high linkage disequilibrium with the four SNPs that we identified in the VDR binding regions of the 17q12-21.1 loci (Fig. 1c). Importantly, in both the 17q12-21.1 and 17q21.2 regions, the VDR binding sites coincide with CTCF and IKZF3 binding sites, as well as H3K27ac peaks indicating active enhancer sites (Fig. 1b and Extended Data Fig. 1b). In particular, the two enhancer sites in 17q12-21.1 (GH17J039753 and GH17J039859) were both predicted to interact with the *ORMDL3* promoter region (Fig. 1b), and the enhancer site in 17q21.2 (GH17J042576) was predicted to interact with the *STAT5A* promoter region (Extended

114 Data Fig. 1b). This suggests a similar mechanism to the one described in [4], whereby
115 SNPs in LD with each other in these enhancer sites affect VDR and CTCF binding, the
116 co-dependence of which in turn could modulate *ORMDL3* and *STAT5A* expression.
117 Although it has been shown that CTCF binding sites can be vitamin D-sensitive[15], no such
118 sites were found in our genomic regions of interest (Fig. 1b and Supp. Fig. 1b).
119
120 Next, we investigated cord blood gene expression data in the Vitamin D Antenatal Asthma
121 Reduction Trial (VDAART) (see Methods) and looked at the genes of interest in the 17q12
122 and 17q21 regions and their interaction with cord blood vitamin D levels as predictors of
123 asthma/wheeze risk at age 3 year of age. After adjusting for relevant covariates (see
124 Methods), the baseline expression term of *IKZF3* was not found to be significantly
125 associated with asthma risk, while the interaction between vitamin D and *IKZF3* was
126 statistically significant (p-val. < 0.05), suggesting that the association of *IKZF3* expression
127 with asthma risk was mediated by vitamin D levels in the cord blood (Extended Data Table
128 1).
129
130 Based on our bioinformatic analysis of the Chr17q12 and 17q21 regions, we hypothesize
131 that low vitamin D tissue levels is associated with decreased *IKFZ3* expression and
132 increased expression of *ORMDL3*, *STAT3*, *STAT5A*, *STAT5B*, and *IL2*.
133
134 **Vitamin-D receptor (VDR) is expressed in Th2 cells in allergic airway inflammation**
135 To test our hypothesis of vitamin D activity at the Chr17q12-21 locus we utilized a mouse
136 model of allergic airway inflammation and identified vitamin D responsive leukocyte
137 subsets in house dust mite (HDM)-sensitized and challenged mice using flow cytometry
138 (Fig.2a, Extended Data Fig. 2a-c). VDR expression was significantly induced in HDM
139 sensitized and challenged mice and almost absent in leukocytes isolated from control
140 (vehicle) lungs (Extended Data Fig. 2c) but. Within the CD45+ population, VDR
141 expression was high in CD4+ T cells (p= 0.0357), while only very few CD8+ T cells and
142 CD19+ B cells expressed VDR (Fig. 2b, Extended Data Fig. 2c HDM). Within the CD4+
143 T cell population, highest VDR expression was detected in Gata3+ Th2 cells (p= 0.002
144 vs Tbet+ and p< 0.0001 vs Foxp3+ T cells). VDR expression was very low in Tbet+ Th1

145 and CD4+ Foxp3+ Treg cells (Fig. 2b). The differential expression of VDR in Th2 cells
146 was further validated by western blot analysis using naïve CD4+ T cells immediately after
147 isolation (0hrs), after activation with CD3/CD28 for 48 hrs and in *in vitro* polarized Th1,
148 Th2 and iTreg cells with well-defined culture conditions (Extended Data Fig. 3a, see
149 Methods section). VDR expression appeared as early as day 1 of Th2 culture conditions
150 and gradually increased during the polarization process (Extended Data Fig. 3b). In the
151 absence of the VDR ligand vitamin D, VDR expression localized to the cytoplasm of Th2
152 cells. Addition of the VDR ligand calcitriol led to a strong translocation of VDR into the
153 nucleus, suggesting functionality of the expressed receptor in the presence of its ligand
154 (Extended Data Fig. 3c). These results identify Th2 cells as vitamin D targets in allergic
155 airway inflammation.
156
157 **Vitamin D status regulates the expression of key genes on Chromosome17q12-21.1**
158 **and Chr17q21.2**
159 Taking cell type specific gene expression and selective expression of VDR in Th2 cells
160 into account, we next analyzed the expression of genes encoded on Chr17q12-21.1 and
161 17q21.2 loci in WT and vitamin D deficient Th2 cultures as well as in Th2 cells post
162 calcitriol stimulation.
163 Vitamin D deficiency differentially regulated the expression levels of several Chr17q12-
164 21.1 encoded genes, with lower expression of *Ikzf3*, *Ormdl3* and *Gsdma* (all p=0.0286)
165 (Fig. 2d). Conversely, stimulation with calcitriol induced the expression of the same genes
166 (all p=0.043) (Fig. 2e). Expression of the Chr17q21.2 genes *Stat3*, *Stat5a* and *Stat5b* was
167 not affected by vitamin D deficiency (Fig.2f). However, after calcitriol stimulation *Stat5a*
168 (p=0.0082) and *Stat5b* (p=0.003) genes were strongly suppressed and *Stat3* (p= 0.0048)
169 expression was increased in Th2 cells. (Fig. 2g). These results hint to a protective role of
170 vitamin D in allergic airway inflammation, by regulating the expression of the IL-2
171 downstream signaling molecules *Stat5a* and *Stat5b*.
172
173 **Deficiency in vitamin D signaling augments allergic airway inflammation**
174 To decipher the protective role of vitamin D signaling in allergic airway inflammation, we
175 employed vitamin D deficient and $VDR^{-/-}$ mice (Fig. 3a) [16]. HDM sensitization of vitamin D

176 deficient mice led to a stronger reaction to the allergen resulting in more prominent peri-
177 bronchial and perivascular leukocytic infiltrates (Fig. 3b). This phenotype was
178 accompanied by lower VDR expression in CD4+ T cells isolated from HDM-exposed
179 lungs compared to WT (Fig. 3c). Vitamin D deficiency led to a robust increase in total
180 immunoglobulin (Ig)E levels (Fig. 3d). Histological findings were associated with higher
181 total BAL leukocyte (p= 0.0008) (Fig. 3e), eosinophil (p= 0.0002) (Fig. 3f) and lymphocyte
182 (p= 0.0023) (Fig. 3g) numbers in vitamin D deficient mice. Th2 cell numbers (p= 0.0127)
183 were also higher in the HDM exposed mice (Fig. 3h) in a manner that was independent
184 of T helper cell skewing (Extended Data Fig. 4a, b). Differentiation and recruitment of
185 Th17 and IL-10 producing CD4+ T cells was not affected by vitamin D deficiency
186 (Extended Data Fig. 4a, b). To validate these findings from vitamin D deficiency, we next
187 employed $VDR^{-/-}$ mice (see Methods). As with the vitamin D deficient mice, HDM
188 sensitization and challenge of $VDR^{-/-}$ mice led to an increased Th2 immune response. The
189 lung phenotype in the $VDR^{-/-}$ mice was marked by dense leukocytic infiltrates around and
190 mucus plugs in the airways (Fig. 3b). The augmented systemic and local immune
191 response increased total IgE titers (p= 0.0489), and total BAL (p< 0.0001 vs WT HDM
192 and p= 0.003 vs Vit D deficient HDM), eosinophil (p< 0.0001 vs WT HDM and Vit D
193 deficient HDM), total lymphocytes (p=0.0194 vs WT HDM and p= 0.0421vs Vit D deficient
194 HDM) and Th2 cells (p= 0.0009 vs WT HDM) (Fig. 3. d-h). $VDR^{-/-}$ did not significantly
195 affect recruitment of Treg and Th17 cells (Extended Data Fig. 4a, b).
196
197 To explore the mechanisms underlying the augmented Th2-phenotype in the lungs of
198 vitamin D deficient and $VDR^{-/-}$ mice after HDM allergen challenge, we analyzed the
199 transcriptional profiles of in vitro polarized Th2 cells from WT and vitamin D deficient mice
200 (Fig.3i). Differential expression and enrichment analysis revealed dysregulation of several
201 pathways implicated in Th2-cell activation, cytokine production, proliferation, and survival
202 with prominent changes in the IL-2/ STAT5 - pathway in vitamin D deficient Th2 cells (p=
203 0.0014) (Fig. 3j, Extended Data Table 2 & 3). The effects of impaired vitamin D signaling
204 on these pathways was confirmed by qRT-PCR and flow cytometry. Baseline expression
205 of IL-2 was markedly increased at both the RNA (p= 0.0286)) and protein levels (p=
206 0.0079) in vitamin D deficient and $VDR^{-/-}$ Th2 cells (Fig. 3k, l). In Vitamin D deficient and

207 VDR$^{-/-}$ Th2 cell *in vitro* incubation, the elevated IL-2 levels were accompanied by a sharp
208 increase in IL-13 production (VitD deficient: $p< 0.0001$; VDR$^{-/-}$: $p= 0.0141$) (Extended Data
209 Fig. 5).
210
211 Taken together, these results indicate a critical role for vitamin D/VDR signaling in
212 regulating type 2 inflammation and identify the IL-2/ Stat5 pathway as a downstream
213 target of vitamin D in Th2 cells.
214
215 **Vitamin D suppresses the activation of the IL-2/Stat5 pathway and cytokine**
216 **production in Th2 cells**
217 To ascertain the vitamin D dependent regulation of the IL-2/Stat5 pathway and the impact
218 on the effector program of Th2 cells, we first analyzed the transcriptional profile of WT
219 Th2 cells exposed to calcitriol during differentiation (Fig. 4a). Gene ontology enrichment
220 analysis of biological processes revealed regulation of several processes impacting
221 inflammatory responses, including chemotaxis and activation of cells (Extended Data
222 Table 4). Calcitriol stimulation of Th2 cells affected several immune related disease
223 pathways, including asthma (Extended Data Fig. 6, Extended Data Table 5). Gene set
224 enrichment analysis (GSEA), performed on the differentially expressed genes,
225 highlighted the negative regulation of IL-2/Stat5 pathway in Th2 cells by calcitriol (Fig. 4b,
226 Extended Data Table 6). Calcitriol stimulation suppressed the expression of *Il2*
227 ($p<0.0001$), *Stat5a* ($p<0.0008$) and *Stat5b* ($p<0.0008$) genes (Fig. 4c). Concordantly,
228 levels of activated Itk (phospho-Itk) ($p= 0.029$) and expression of the IL2Rβ (CD25) ($p=$
229 0.0441) were reduced on a per cell basis (Fig. 4d).
230
231 Next, the impact of calcitriol stimulation on the effector function of Th2 cells was assessed
232 by flow cytometric analysis for the T2 cytokine IL-13. Activation of the vitamin D/VDR
233 pathway led to significant suppression of IL-13 production in CD4+ T cells ($p= 0.0012$)
234 (Fig. 4e).
235
236 To further delineate the molecular impact of vitamin D on Th2 cell biology, we integrated
237 the murine transcriptional profile with a recently developed human Protein-Protein

238 Interaction (PPI) database[17] . By modeling the signal transduction process as a sequential
239 path on the PPI network that starts from a receptor and propagates downstream to a
240 transcription factor via multiple intermediate proteins (for details see Methods section,
241 Extended Data Fig. 7a), we inferred the active signaling flow in Th2 cells for control
242 (vehicle) and calcitriol stimulated Th2 cells. As input of our network analysis, we selected
243 a subset of receptors and transcription factors that are known to be involved in CD4+ T
244 cell activation, Th2 cell differentiation, and cytokine production (Extended Data Table 7).
245 For clarity of the figure, we display the gene names. Corresponding protein names are
246 attached in Extended Data Table 8. In control Th2 cells, our network analysis revealed
247 the engagement of a variety of receptors including IL4R, IL2RA, CD28, and TNF-
248 receptors. Downstream to these receptors, the most active signaling paths highlighted
249 the activation of STAT3, STAT5A/B, NFkB1, and IKZF1 transcription factors (Extended
250 Data Fig. 7b) via multiple adapter proteins of the TRAF and JAK family. Interestingly,
251 these transcription factors are known to be involved in differentiation and activation
252 pathways in Th2 cells Conversely, after calcitriol stimulation, signal from IL4R, CD28 and
253 TNFSF8 propagated over different interaction partners (Fig. 4f). Calcitriol specific edges
254 are highlighted in orange color. Molecular mediators included the cytoskeletal proteins
255 VAV1 and RACK1 and emphasized activation of the transcription factors AP-1
256 (FOS/JUND dimer) and NFATC1.
257 Our network analysis highlighted a central role of the transcriptional repressor IKZF1
258 (IKAROS) upon calcitriol stimulation, which was targeted by multiple downstream
259 mediators including IKZF3 (AIOLOS). Notably, the IKZF3 gene encodes for the AIOLOS
260 protein, a direct interaction partner of the IKZF1-encoded IKAROS. Both transcription
261 factors, as homo- and heterodimers, suppress IL-2 expression on the transcriptional
262 levels in mouse and human lymphocytes[18]. Calcitriol increased the number of edges
263 connecting intermediate proteins to the transcriptional repressor IKAROS. Among the
264 connecting proteins, AIOLOS interaction with IKAROS was implicated in repression of IL-
265 2 expression in Th2 cells by vitamin D. Absence of STAT5A/B mediators in the active
266 signaling paths of calcitriol stimulated Th2 cells further suggested repression of the Th2
267 cell STAT5 pathway with calcitriol compared to control (Extended Data Fig. 7b).
268

269 Taken together, these results indicate that the specific suppression of the IL-2/Stat5
270 pathway by vitamin D results in reduced cytokine production by Th2 cells. Our findings
271 suggest that this suppression was mediated by the vitamin D dependent regulation of
272 IKAROS (IKZF1) through the induction of AIOLOS (IKZF3).
273
274 **Vitamin D supplementation alleviates the allergic phenotype in the lung by**
275 **suppressing type 2 cytokine production in a dose dependent manner**
276 To test if vitamin D supplementation prevents the development of T2 driven allergic
277 inflammation in the lung, custom rodent diets with select vitamin D doses were used: 400
278 IU/kg chow (400 IU; low), 1000 IU/kg chow (1000 IU; regular) and 4000 IU/kg chow (4000
279 IU; high) (see Methods section). The 1000 IU group was used as the control group, as it
280 contains the average amount of vitamin D fortified in standard rodent chow. HDM
281 exposure led to recruitment of leukocytes into the lung tissue and BAL (Fig. 5a, b), with a
282 predominant eosinophilic and lymphocytic infiltrate as well as high numbers of IL-13+ Th2
283 cells (Fig. 5c-e). There were trends for higher cellular infiltration in the airways when mice
284 were supplemented with the low vitamin D doses (400 IU), but these inflammatory
285 responses were not significantly different from the phenotype observed with 1000 IU.
286 Lung and airway pathology were similar between these dosing groups, with similar
287 numbers and frequencies of the different leukocyte populations. In sharp contrast, dietary
288 supplementation with the higher vitamin D dose (4000 IU) decreased the inflammatory
289 phenotype in HDM exposed mice compared to the 400 IU and 1000 IU dosed animals.
290 Concordant with the histological findings, BAL leukocytes ($p< 0.0001$) were decreased
291 with marked reductions in BAL eosinophil ($p=0.0016$) and lymphocyte numbers ($p=0.026$)
292 (Fig. 5c-d), and the frequency of IL-13+ Th2 cells was significantly reduced in the lungs
293 with 4000 IU of vitamin D ($p= 0.0066$ vs 400 IU HDM; $p=0.0011$ vs 1000 IU HDM) (Fig.
294 5e). Of note, dietary supplementation with high vitamin D levels, increased VDR
295 expression in CD4+ T cells from HDM exposed lungs ($p< 0.0001$) (Extended Data Fig.
296 8b).
297
298 To ascertain that dietary supplementation with vitamin D specifically altered mouse Th2
299 cell differentiation and the effector program, splenic naïve CD4+ T cells from 400 IU and

300 4000 IU mice were studied. Of interest, naïve CD4+ T cells did not express VDR until
301 they were exposed to Th2 polarizing conditions. Gata3 expression on per cell basis was
302 lower in 4000 IU Th2 cells (p= 0.0286) (Extended Data Fig. 9a). This was accompanied
303 by higher VDR protein expression (p= 0.0286) (Extended Data Fig. 9b). The expression
304 of IL-2 (p= 0.0004) and the Th2 cytokines IL-13 (p= 0.0159) and IL-5 (p= 0.0159) were
305 lower in 4000 IU Th2 cultures (Extended Data Fig. 9c-f).
306
307 To explore the specific induction of Aiolos expression for vitamin D mediated suppression
308 of IL-2 production in Th2 cells, Aiolos expression was monitored throughout Th2
309 differentiation. Aiolos expression gradually increased under Th2 polarizing conditions in
310 CD4+ T cells, starting as early as day 1 of in vitro culture (Fig. 5f). Simultaneous exposure
311 to calcitriol further increased Aiolos protein levels compared to vehicle in Th2 cells (p=
312 0.0079) (Fig. 5g).
313
314 To test if vitamin D exerts its inhibitory effect on IL-2 production via Aiolos induction, Ikzf3^{-}
315 $^{/-}$ mice were employed, exposed to Th2 polarizing conditions and assessed for IL-2
316 production after calcitriol exposure. IL-2 production in control Ikzf3$^{-/-}$ Th2 cultures was
317 significantly higher compared to WT Th2 cells. Calcitriol significantly reduced IL-2 levels
318 in both, WT (p= 0.0001) and Ikzf3$^{-/-}$ Th2 cells (p= 0.0001) (Fig. 5h); however, the
319 suppressive effect of calcitriol on IL-2 production was significantly higher in WT Th2 cells
320 (~ 65% inhibition) compared to Ikzf3$^{-/-}$ Th2 cells (~40% inhibition) (p= 0.0001) (Fig. 5h).
321
322 Taken together, these results indicated that vitamin D can regulate Aiolos expression and
323 suggested a role for Aiolos as a downstream effector for selectively fine-tuning Th2 cell
324 IL-2 production by vitamin D.
325
326 **Discussion**
327 We utilized human genetics to identify SNPs on chromosome 17q12-21.1 and 17q21.2
328 that were within GWAS regions for Th1 and Th2 autoimmune diseases. Of note, many of
329 these SNPs were within VDR binding sites. We then determined by eQTL analysis of the
330 genes in these two genomic regions that IKZF3 expression was controlled by four cis-

331 eQTLs in the enhancer region targeting ORMDL3 and IKZF3, and in the enhancer region
332 targeting ORMDL3, GSDMA and GSDMB. Next, we demonstrated that two SNPs in
333 CTCF binding sites were in strong LD with these 4 eQTL SNPs and that the two enhancer
334 sites in 17q12-21.1 were both predicted to interact with the ORMDL3 promoter region,
335 and the enhancer site in 17q21.2 was predicted to interact with the STAT5A promoter
336 region thus, suggesting a plausible human molecular genetic mechanism by which
337 vitamin D could activate IKZF3 to repress ORMDL3 and immune system development.
338 Finally, we leveraged bulk RNAseq in the cord blood of the VDAART trial to show that an
339 interaction for vitamin D level and IKZF3 expression that was associated with reduced
340 asthma risk at 3 years of age.
341
342 The vitamin D receptor was genetically associated with asthma in 2004[19] and high intake
343 of vitamin D by pregnant women is associated with about a 50% reduction in asthma risk
344 in the mother's offspring[15,20]. Together, these exciting findings led to a comprehensive
345 theory about how vitamin D deficiency could influence asthma occurrence through its
346 effects on lung and immune system development and that progressive decreases in
347 vitamin D intake from 1946 onward could be contributing to the epidemic of allergic and
348 autoimmune diseases[1]. Vitamin D deficiency is the most common vitamin deficiency in
349 the world today and is particularly prevalent in pregnant women where the fetal lung and
350 immune system are developing[21–23].
351
352 To determine the impact of vitamin D supplementation, we performed a clinical trial, the
353 Vitamin D Antenatal Asthma Trial (VDAART) in pregnant women who either had allergies
354 or asthma or had family members with these conditions. The participants were given
355 either 4400 IU of vitamin D3 or 400 IU and were followed throughout their pregnancy and
356 for the first six years of the life of the child[24]. The results of the trial were not statistically
357 significant using conventional intent to treat analysis[25,26] but the reasons were complex,
358 as is often seen when the effects of nutrients are studied. Most importantly, unlike
359 conventional drug trials where one compares drug to no drug or alternative drug, in
360 nutrient trials there is nutrient already present in the placebo group. This creates
361 misclassification that can reduce trial power. When we performed a meta-analysis of the

362 two pregnancy related trials of vitamin D, we got a statistically significant reduction in
363 asthma in the offspring of women who had the higher vitamin D intake during pregnancy
364 and, when we adjusted for the baseline level of vitamin D in the meta-analysis, we got a
365 reduction in asthma risk of 50 percent, exactly what we saw in the observational studies
366 performed previously[27,28].
367
368 To link the results of the VDAART trial directly to the chr17q12 locus we genotyped SNP,
369 rs12936231, in ZPBP2, the gene adjacent to ORMDL3, and stratified the VDAART trial
370 results by maternal genotype at this locus and found that the vitamin D effect in the trial
371 was significantly influenced by genotype with the GG genotype exhibiting a protective
372 effect on asthma risk in the child and the CC or GC genotype not being responsive to
373 vitamin D, additionally this result was related to sphingolipid production with the children
374 protected from asthma having higher sphingolipid production[3].
375
376 This SNP (rs12936231) is one of two SNPs (the other being rs4065275) that alter the
377 chromatin state of a regulatory domain, specifically two CTCF binding sites, in the
378 chr17q12-21.1 locus that are correlated with the expression of ORMDL3[4,14]. 4C-seq
379 assays previously demonstrated that the ORMDL3 promoter interacts with a long-range
380 enhancer in IKZF3 that promotes (or represses) transcription of ORMDL3 in cells
381 expressing both genes and the binding of CTCF per the G allele of rs12936231 in ZPBP2
382 blocks this interaction resulting in reduced transcription of ORMDL3 on haplotypes with
383 the rs12936231-G allele[4]. If rs12936231 is not activated then there is activation of the
384 other CTCF binding site (rs4065275) intronic to ORMDL3 thus favoring the expression of
385 ORMDL3 and increased asthma risk[4].
386
387 Mouse models have contributed to our understanding of ORMDL3 function as mice
388 expressing the ORMDL3 transgene exhibit spontaneous increases in airway hyper
389 responsiveness, the essential feature of asthma. This increase in AHR was associated
390 with airway remodeling and peri bronchial fibrosis without airway
391 inflammation[29]. ORMDL3 is pleotropic, influencing Ca++ signaling, and the unfolded
392 protein response. Most importantly, increased expression of ORMDL3 inhibits the

393 enzyme serine palmityl-transferase, the rate limiting step in the production of
394 sphingolipids and ORMDL3 TG mice have reduced levels of sphingolipids[30]. What has
395 been unclear is how ORMDL3 is controlled.
396
397 To confirm our human molecular genetic findings, we chose to utilize mouse models of
398 allergic lung inflammation. We show strong VDR expression in CD4+ Th2 cells and
399 alterations in chr17q12-21.1 and 17q21.2 gene expression induced by vitamin D status.
400 Expression of VDR has been reported for airway epithelial cells and different immune cell
401 types present in the lung[31]. In lymphocytes, *ex vivo* and *in vitro* studies describe low
402 baseline VDR transcript expression levels that were transiently increased by activating
403 signals and calcitriol stimulation[32]. Here, we report a differential VDR expression pattern
404 in CD4+ T cell subsets in allergic inflamed lungs and post lineage specific cytokine
405 stimulation *in vitro*, with strongest expression in Th2 cells. Activation of VDR suppressed
406 IL-2, IL-5, and IL-13 production by Th2 cells. The expression of VDR in Gata3+Th2 cells
407 in the lung might represent an endogenous control mechanism to curb the pathogenic
408 cell activity and cytokine production after repetitive allergen contact. *Ex vivo* and *in vitro*
409 Th1, nTreg and iTreg cells expressed low VDR protein levels at baseline. It remains to be
410 determined whether other Th-subsets described in allergic inflammation express VDR at
411 baseline and if either calcitriol or other secondary signals, specific for each subset, could
412 induce VDR expression during inflammation.
413
414 Vitamin D deficiency that had been introduced over two generations and impaired vitamin
415 D signaling led to an augmented allergic phenotype in the lung after allergen exposure
416 with a dominating Th2-signature locally and systemically. This had likely been due to
417 specific deregulation of Th2 cells instead of Th cell skewing, since neither Th17 nor Treg
418 development and recruitment had been significantly affected. In contrast, in mice
419 supplemented with high vitamin D doses over two generations, VDR expression and
420 consequently vitamin D responsiveness was higher in CD4+ T cells from the animals'
421 lungs, almost abrogating the inflammatory process in the lung after allergen challenge.
422 While the vitamin D dose had been chosen to replicate the VDAART trial in the mouse,
423 the duration of supplementation was adopted to the protocol of generating vitamin D

424 deficient mice. Both factors might influence the outcome here compared to prior rodent
425 studies with inconclusive results.
426
427 Differentiation of Th2 cells is driven by IL-4 induced Gata3 expression in naïve CD4+ T
428 cells. This process depends on a positive feedforward loop by IL-2 and its downstream
429 STAT5 signaling pathway for the effective expression of IL-4[33]. Therefore, either
430 interfering with Gata3 expression or the IL-2 pathway represents a promising strategy to
431 finetune Th2-driven immunity. Our data highlight the specific regulation of the IL-2/STAT5
432 pathway by vitamin D. Vitamin D deficiency and impaired VDR signaling caused elevated
433 IL-2 production by Th2 cells, mounting in high IL-13 production. Elevated IL-13 levels *in*
434 *vivo*, could amplify the local T2 responses in the lung. In sharp contrast, exposure of
435 polarizing Th2 cells to calcitriol was able to suppress IL-2 production, expression and
436 activation of STAT5A/B and therefore IL-13 production by Th2 cells. The transcription
437 factor AIOLOS has previously been shown to suppress IL-2 expression on the
438 transcriptional level[18]. We report here a vitamin D mediated induction of Aiolos expression
439 in Th2 cells, which is impaired by vitamin D deficiency. High Aiolos expression coincided
440 with lower IL-2 production, ameliorated STAT5A/B expression, and IL-13 production in
441 Th2 cells. *In vitro* Th2 polarization of naïve CD4+ T cells isolated from mice supplemented
442 with higher vitamin D levels, without further exogenous calcitriol stimulation, developed a
443 weakened Th2 phenotype, characterized by lower IL-2, IL-5, and IL-13 production. Since
444 naïve CD4+ T cells do not express VDR, these results implicate changes in chromosomal
445 accessibility by high vitamin D in the developing immune system, which needs further
446 investigation.
447
448 Experiments here with Ikzf3$^{-/-}$ mice demonstrated significant reductions in vitamin D
449 mediated control of Th2 cell cytokine production, but the vitamin D response was not
450 completely impaired, suggesting additional mechanisms for vitamin D regulation of Th2
451 cells – several possibilities were uncovered by our PPI analyses. These will be the subject
452 of future research. In addition, we only investigated a Th2 mouse model of asthma and
453 have not extended our mouse work to Th1 models of autoimmunity. We have still to
454 consider other genes that might be linked to these two genetic loci and there are likely

455 other VDR binding sites of importance in both asthma and Th1 autoimmunity. More work
456 to determine the exact levels of vitamin D that confer this protective effect would also be
457 worthy of further investigation.
458
459 In summary, we have leveraged clinical trial data, molecular genetic bioinformatic data
460 and mouse model data to outline for the first time, a comprehensive molecular genetic
461 mechanism for how vitamin D influences not only asthma, but both Th1 and Th2
462 autoimmune disease. The significance of these findings relates to the high prevalence of
463 vitamin D deficiency, especially during pregnancy, and the strong possibility that the
464 epidemic of asthma and autoimmunity might be significantly reduced if vitamin D levels
465 were elevated worldwide.
466
467
468 **Figure Legends**
469 **Figure 1. VDR binding sites on Chr17q12 and q21.1 overlap with open chromatin**
470 **signatures. a,** Significant disease, and trait associations in 17q12-21.1 (y-axis), retrieved
471 from the NHGRI-EBI GWAS Catalog, with at least one significant SNP (x-axis) in
472 Chr17q12-21.1. Colored bars denote autoimmune diseases mapped to Th1 (red bars) or
473 Th2 (blue bars) driven immunity. **b,** University of California Santa Cruz (UCSC) Genome
474 Browser tracks showing chromosomal location, common dbSNPs, VDR-, RXR-, CTCF-
475 and IKZF3-binding sites and H3K27Ac marks present in the Chr17q12-21.1 locus. VDR
476 binding sites overlapping with active regulatory elements are highlighted by colored
477 boxes. **c**, Linkage disequilibrium (LD) between the significant SNPs in the Chr17q12-21.1
478 (magenta) and 21.2 (green) region, highlighting Th1/Th2-associated SNPs (red and blue,
479 respectively), eQTLs in the VDR binding regions in Chr17q12-21.1 and 21.2 (yellow), and
480 functional asthma SNPs from the literature (cyan).
481
482 **Figure 2. VDR expression is elevated in Th2 cells and vitamin D regulated**
483 **expression of genes on Chr1q12 and Chr17q21. a,** Scheme of the house dust mite
484 (HDM) induced airway inflammation protocol. **b,** Flow cytometric analysis and cell
485 frequencies of VDR expression in CD45+ CD4+ T cells in the respective groups (n=4-5).

486 **c**, Flow cytometric analyses and cell frequencies of VDR expression in Th1 (Tbet+), Th2
487 (Gata3+) and Treg (Foxp3+) cells in the respective groups (n=4-7). Quantitative RT-PCR
488 analysis of relative mRNA expression levels of genes encoded on Chr17q12-21.1 in Th2
489 cultures of WT and vitamin D deficient mice (**d**) and control and calcitriol stimulated
490 cultures (**e**). Quantitative RT-PCR analysis of relative mRNA expression levels of genes
491 encoded on Chr17q21.2 in Th2 cultures of WT and vitamin D deficient mice (**f**) and control
492 and calcitriol stimulated cultures (**g**). Gene expression levels were normalized to the
493 house keeping gene *L32* and are expressed relative to the expression level in WT (**d, f**)
494 or WT-vehicle (**e, g**) Th2 cells. (n ≥ 4 per group). Each symbol represents one mouse.
495 Numbers in flow plots indicate percentages. Error bars indicate the s.e.m. Statistical tests:
496 two-tailed Mann-Whitney U test (**b, c**). *P < 0.05, **P < 0.01, ***P < 0.001. Data
497 summarize results from two independent experiments.
498
499 **Figure 3. Vitamin D deficiency augments allergic airway inflammation. a,** Schematic
500 presentation of the different mouse strains used. **b,** Representative H&E-stained lung
501 sections from saline and HDM-exposed wild type (C57/BL6; WT), vitamin D deficient and
502 $VDR^{-/-}$ mice (x 10 magnification). Black arrows point to the peri bronchial infiltrate. **c,**
503 Representative flow plots assessing VDR expression in lung CD4+ T cells from the
504 indicated groups. **d,** Total IgE levels detected in the sera of respective groups. **e- g,**
505 Absolute numbers of leukocytes (**e**), eosinophils (**f**) and lymphocytes (**g**) in the airways of
506 the respective groups. **h**, Frequencies of IL-13 producing Th2 in the lung. **i,** Heat map
507 showing differentially expressed genes between WT and vitamin D deficient Th2 cultures
508 identified by RNA-Sequencing analysis. Analysis and visualization were performed with
509 DESeq2. **j**, Overrepresentation analysis of Hallmark gene sets in the differentially
510 expression gene set. The x-axis represents the gene ratio in the respective gene set. Dot
511 sizes denote the number of genes in the respective pathway. The dot color indicates the
512 FDR-adjusted p-value. Analysis and visualization were performed with the clusterProfiler
513 package. **k,** Quantitative RT-PCR analysis of *Il-2* mRNA expression in Th2 cultures from
514 the respective groups (n=4 per group). Gene expression levels were normalized to the
515 house keeping gene *L32* and are expressed as fold-induction compared to WT Th2 cells.
516 **l**, Flow cytometric analysis and cell frequencies of IL-2 production in WT and $VDR^{-/-}$ Th2

517 cultures (n=5 per group). Each symbol represents one mouse. Error bars indicate the
518 s.e.m. Statistical significance was determined with: Mixed-effect analysis with Holm-
519 Šidák's post-hoc analysis (**d –h**), two-tailed Mann-Whitney U test (**k, l**). *P < 0.05, **P <
520 0.01, ***P < 0.001, ****P < 0.0001. Data summarize results from two or three independent
521 experiments with n>8 per group.
522
523 **Figure 4. Vitamin D stimulation of polarizing Th2 cells suppresses the IL-2/Stat5**
524 **pathway. a**, Heat map of differentially expressed genes between vehicle (EtOH [% v/v])
525 and calcitriol treated WT Th2 cells. Analysis and visualization were performed with
526 DESeq2. **b**, Gene set enrichment analysis (GSEA) of differentially expressed genes.
527 Analysis and visualization were performed with the clusterProfiler package. **c**,
528 Quantitative RT-PCR for *Il-2*, *Stat5a* and *Stat5b* mRNA expression in Th2 cells exposed
529 to either vehicle or calcitriol. Gene expression levels were normalized to the house
530 keeping gene *L32* and are expressed as fold-induction compared to control cells. **d**, Flow
531 cytometric analysis and mean fluorescence intensities of Itk and Il2rβ expression in
532 indicated groups. **e**, Flow cytometric analysis and quantification of IL-13 expression in
533 respective groups. **f**, Network analysis to visualize vitamin D induced molecular changes
534 in the molecular interactome of calcitriol stimulated CD4+ Th2. Predefined set of cell
535 membrane receptors were set as starting points (orange nodes) and annotated
536 transcription factors were set as ending points (blue). All intermediate proteins on the PPI
537 are visualized as grey nodes. Molecular interactions only overrepresented in calcitriol
538 stimulated cells are shown as orange arrows. Each symbol in the bar graphs represents
539 one individual sample and data summarize the results from two or three independent
540 experiments with n≥ 5. Error bars indicate the s.e.m. Statistical test: two-tailed Student's
541 t-test (**c, e**) and two-tailed Mann-Whitney U-test (**d**). *P < 0.05, **P < 0.01, ***P < 0.001.
542
543 **Figure 5. Prenatal vitamin D supplementation protects from asthma development.**
544 **a,** H&E staining of representative lung sections of indicated experimental groups.
545 Arrowheads point to peri bronchial infiltrates. **b-e,** Absolute numbers of total BAL
546 leukocytes (**b**), eosinophils (**c**), lymphocytes (**d**) and lung IL-13+ Th2 cells (**e**). **f**, Flow
547 cytometric analysis of Aiolos expression in differentiating Th2 cells at indicated time

548 points. **g**, QRT-PCR analysis of *Ikzf3* transcripts in respective groups. Expression levels
549 were normalized to the house keeping gene *L32* and are expressed as fold change
550 expression over the control samples WT-vehicle/ WT. **h**, Flow cytometric analysis of
551 Aiolos expression in control and calcitriol stimulated Th2 cells. **i**, Flow cytometric analysis
552 and frequencies of IL-2+ cells in WT and Ikzf3$^{-/-}$ cultures post indicated treatment. Each
553 symbol represents and independent sample (n= 9 per group). Flow cytometric analysis
554 and quantification of VDR expression in lung CD4+ T cells of the respective groups. Each
555 symbol represents one individual mouse and data summarize the results from two to three
556 independent experiments with n>8 per group. Error bars indicate the s.e.m. Statistical
557 significance was determined with Mixed-effect analysis with Holm-Šidák's post-hoc
558 analysis (**b-e**), two-tailed Mann-Whitney U-test (**g, h**) and One-way ANOVA with Holm-
559 Šidák's post-hoc analysis (**g**). *P < 0.05, **P < 0.01, ***P < 0.001, ****P < 0.0001.
560
561 **Extended Data Figure 1: a,** Significant disease and trait associations in 17q21.2 (y-axis),
562 retrieved from the NHGRI-EBI GWAS Catalog, with at least one significant SNPs (x-axis)
563 in Chr17q21.2. Colored bars denote autoimmune diseases mapped to Th1 (red bars) or
564 Th2 (blue bars) driven immunity. **b,** University of California Santa Cruz (UCSC) Genome
565 Browser tracks showing chromosomal location, common dbSNPs, VDR-, RXR-, CTCF-
566 and IKZF3-binding sites and H3K27Ac marks present in the Ch17q21.2 locus. VDR
567 binding sites overlapping with active regulatory elements are highlighted by colored
568 boxes.
569
570 **Extended Data Figure 2. Baseline VDR expression is confined to the CD4+ Foxp3-**
571 **Teff cell population. a**, Gating strategy for the analysis of VDR expression in different
572 leukocyte populations in the lung. **b,** Flow cytometric analysis and cell frequencies of VDR
573 expression in CD45+, CD4+, CD8+ and CD19+ in the respective groups (n=4-5). **c**,
574 Representative flow plots of lung CD45+ CD4+ T cells isolated from saline and HDM-
575 immunized and -challenged mice for the co-expression of Foxp3 and VDR. Each symbol
576 represents one mouse. Numbers in flow plots indicate percentages. Error bars indicate
577 the s.e.m. Statistical tests: two-tailed Mann-Whitney U test. *P < 0.05. Data summarize
578 results from two independent experiments.

579

580 **Extended Data Figure 3. VDR expression is induced during CD4+ Th2 cell**
581 **differentiation. a**, Representative immunoblot for VDR expression in freshly isolated (0
582 hrs) and activated CD4+ CD62L+ CD44- naïve T cells (48 hrs.) and *in vitro* polarized Th1,
583 Th2 and iTreg cells. Kidney samples of WT and $VDR^{-/-}$ mice were used as controls. **b**,
584 Representative immunoblot for VDR expression in polarizing Th2 at the indicated days of
585 *in vitro* culture. **c**, Representative image of VDR localization in *in vitro* polarized Th2 cells
586 stimulated with vehicle (EtOH, [% v/v]) or calcitriol.

587

588 **Extended Data Figure 4. Vitamin D deficiency does not alter CD4+ IL-10 and IL-17A**
589 **expression allergic airway inflammation.** Frequencies of IL-10 (**a**) and IL-17A (**b**)
590 CD4+ T cells. Each symbol represents one mouse. Error bars indicate the s.e.m. Data
591 summarize results from two or three independent experiments with n>8 per group.

592

593 **Extended Data Figure 5.** Flow cytometric analysis and frequencies of IL-13 expression
594 in WT, vitamin D deficient and $VDR^{-/-}$ Th2 cultures (n=5-9 per group). Each symbol
595 represents one individual sample and data summarize the results from two or three
596 independent experiments. Error bars indicate the s.e.m. Statistical tests: Kruskal- Wallis
597 Test with Dunn's post-hoc analysis. *P < 0.05, **P < 0.01, ****P < 0.0001.

598

599 **Extended Data Figure 6. KEGG pathways analysis post vitamin D stimulation.** List
600 of KEGG pathways enriched (p-adj. < 0.05) in DE genes after calcitriol stimulation. The
601 x-axis indicates the number of genes annotated to each pathway. The bar colors indicate
602 the FDR-adjusted p-value based on the colormap on the right side of the figure. The R
603 package clusterProfiler was used for the enrichment analysis and visualization.

604

605 **Extended Data Figure 7. Active signaling pathways in Th2 cells. a**, Schematic
606 representation of the network analysis employed. **b**, Network analysis to visualize active
607 signaling paths in control stimulated Th2 cultures. Predefined set of cell membrane
608 receptors were set as starting points (orange nodes) and annotated transcription factors
609 were set as ending points (blue). All intermediate proteins on the PPI are visualized as

610 grey nodes. Molecular interactions only overrepresented in control stimulated cells are
611 shown as purple arrows.
612
613 **Extended Data Figure 8. Prenatal vitamin D supplementation increases VDR**
614 **expression in CD4+ T cells. a**, Schematic presentation of the dietary intervention
615 protocol and breeding scheme with vitamin D. **b**, Flow cytometric analysis and
616 quantification of VDR expression in lung CD4+ T cells of the respective groups. Each
617 symbol represents one individual mouse and data summarize the results from two to three
618 independent experiments with n>8 per group. Error bars indicate the s.e.m. Statistical
619 significance was determined with One-way ANOVA with Holm-Šidák's post-hoc analysis.
620 *P < 0.05, **P < 0.01, ***P < 0.001, ****P < 0.0001.
621
622 **Extended Data Figure 9. Prenatal vitamin D supplementation mitigates Th2**
623 **development and cytokine production *in vitro*. a-g,** Representative flow plots and cell
624 frequencies of (**a**) Gata3, (**b**) VDR, (**c**), IL-2, (**d**) IL-13, (**e**) IL-5 expression in indicated
625 groups. Each symbol represents one individual sample and data summarize the results
626 from two to three independent experiments (n= 4-5 per group). Error bars indicate the
627 s.e.m. Statistical test: two-tailed Mann-Whitney U-test (a – g). *P < 0.05, **P < 0.01, ***P
628 < 0.001.
629
630 Supplementary Figure 1. Uncropped immunoblot shown in Extended Data Fig. 2a
631 Supplementary Figure 2. Uncropped immunoblot shown in Extended Data Fig. 2b
632
633
634 **Methods**
635 *In silico analysis of VDR binding sites on Chr17q12-21*
636 For our *in-silico* analysis, we focused on two genomic regions that are known to harbor
637 variants associated with asthma and autoimmune disease susceptibility. The first one is
638 a 240 kb region that covers parts of the 17q12 and 17q21.1 loci and contains IKZF3,
639 ZPBP2, ORMDL3, GSDMA and GSDMB (chr17: 37,899,254–38,139,253; hg19) and the
640 second one is a 420 kb region in the 17q21.2 locus that includes STAT3, STAT5A and

641 STAT5B (chr17: 40,330,000-40,750,000; hg19). When selecting these genomic ranges,
642 our criterion was to make the window inclusive of any potential enhancer regions targeting
643 the above genes of interest. We used the GeneHancer [34] track in the UCSC Genome
644 Browser (http://genome.ucsc.edu) to determine predicted enhancer-target gene
645 interactions. We obtained VDR, IKZF3, CTCF and Vitamin D-sensitive CTCF binding sites
646 from [35–38], converted their genomic coordinates to hg19 if a different genome build was
647 used in the original publication, and added them as custom tracks on the Genome
648 Browser. We retrieved the known disease and trait associations in these loci from the
649 NHGRI-EBI GWAS Catalog (downloaded on 7/26/2021) [8] and retained all hits that were
650 deemed significant ($p<10^{-5}$). We downloaded significant single-tissue eQTLs for IKZF3
651 and PSMCIP3 in all tissues from the Common Fund (CF) Genotype-Tissue Expression
652 Project (GTEx) Analysis Release V8 (dbGaP Accession phs000424.v8.p2), through the
653 GTEx Portal (https://www.gtexportal.org/home/) in July 2021. We calculated linkage
654 disequilibrium (LD) using the NCI LDmatrix Tool (https://ldlink.nci.nih.gov/?tab=ldmatrix),
655 and by selecting all available populations.
656
657
658 *Gene expression analysis in VDAART cohort*
659 To understand the putative mechanism linking IKZF3 expression and Vitamin D to asthma
660 risk we considered umbilical cord blood (CB) RNA-seq data from the VDAART trial. Total
661 RNA was isolated from cord blood using the QIAGEN PAXgene Blood RNA Kit according
662 to the manufacturer's protocol. Quality was assessed using the Nanodrop 8000
663 spectrophotometer. Sequencing libraries were constructed with the TruSeq® Stranded
664 Total RNA Library Prep Globin Kit (Illumina) and the NEXTflex Small RNA sequencing Kit
665 v3 (Boo Scientific). Sequencing was performed using a NextSeq 550 instrument
666 (Illumina). Trimmed reads were mapped to The GRCh38 reference genome using
667 STAR[39]. Read counts were computed with htseq[40]. The data includes 443 expression
668 profiles of pregnant women with and without asthma undergoing measurements of
669 Vitamin D levels in their CB. Each sample is matched with the observed patterns of
670 wheezing and asthma in the newborn. We filtered all the samples where information about
671 Vitamin D levels, asthma/wheezing patterns or other covariates were missing, obtaining

672 393 expression profiles. Data was normalized with the voom function of the edgeR R
673 package [41], and Vitamin D levels were binarized using 30 ng/ml as threshold. We
674 performed logistic regression of asthma status as a function of the expression levels of
675 IKZF1 and IKZF3, including their interaction term and the interaction between IKZF3 and
676 Vitamin D. Since IKZF3 forms homodimers and heterodimers with IKZF1, we included
677 IKZF1 in the model. We adjusted the model for maternal asthma status and child race.
678
679 *Mice*
680 All animal studies were approved by the institutional animal care committee. Mice were
681 maintained in a virus- and parasite-free animal facility under a 12-h light, 12-h dark cycle.
682 C57BL6/J wild type (WT) mice were bred and housed at the MGH animal facility. Vitamin
683 D-deficient mice (C57BL6/J) were bred and maintained in a UV-free environment and
684 weaned onto a similar diet lacking vitamin D metabolites (TD97340; Harlan Teklad) that
685 results in undetectable circulating 25-hydroxyvitamin D levels[16]. $VDR^{-/-}$ mice ($Vd^{rtm1Mbd/J}$),
686 on C57BL6/J background, were weaned at 18 d on a diet that maintains normal mineral
687 ion homeostasis in the absence of VDR signaling (2% calcium, 1.25% phosphorus, 20%
688 lactose supplemented diet, TD96348; Harlan Teklad, Madison WI)[42].
689
690 BALB/c male and female mice were purchased from Charles River Laboratories at 6–8
691 weeks of age and fed with diets supplemented with varying amounts of vitamin-D3
692 (TD97340 was used as base diet and supplemented with either 400 IU vitamin D/kg, 1000
693 IU vitamin D/kg or 4000 IU vitamin D/kg). Mice were bred on the specific diets for two
694 generations to assure stabilization of vitamin D levels. Resulting F2 litters were used for
695 the experiments. Mice were housed under standard conditions with free access to rodent
696 chow and water. All animal protocols were reviewed and approved by the Harvard
697 Medical School standing committee on animals.
698
699 *House dust mite induced-airway inflammation*.
700 Mice were exposed to D. pteronyssinus extracts (Greer Laboratories, 10.52 EU/mg
701 endotoxin) via the intranasal application of HDM (25 µg in saline) on days 1,2,3, 8 to 15.
702 Control mice received equal volumes of saline (Hospira Inc., Lake Forest, IL, USA).

703 Twenty-four hours after the final challenge, mice were sacrificed, and specimens
704 sampled.
705
706 *Bronchoalveolar Lavage*.
707 Bronchoalveolar Lavage (BAL) was performed with 2 × 1 mL of PBS/0.02% bovine serum
708 albumin (BSA). The total number of leukocytes was determined using a TC20 Automated
709 Cell Counter (BioRad Systems). To differentiate cell types, cytospins were prepared and
710 stained with Kwik-Diff solutions as per manufacturer's instructions (Fisher Scientific) and
711 200 immune cells per slide were counted.
712
713 *Histological staining*
714 Lungs were perfusion fixed with zinc fixative (BD Pharmingen, San Diego, CA) Tissues
715 were paraffin embedded, divided into sections, and stained with hematoxylin and eosin
716 by MGH DF/HCC Specialized Histopathology Services Core Histology Core. After paraffin
717 embedment, 3-μm sections were stained with hematoxylin and eosin.
718
719 *Measurements of serum immunoglobulins*
720 Blood samples were collected 24 hours after the final aerosol challenge and serum was
721 prepared. Total IgE levels were measured by ELISA (Chondrex) according to
722 manufacturer's instructions.
723
724 *Dissociation of mouse tissues, in vitro polarization of CD4 Th-subsets and flow cytometry*
725 *analyses*.
726 Lungs were perfused via the right heart ventricle with PBS, excised, and digested with
727 collagenase D (2 mg/ml; Roche) in RPM 1640 (Sigma-Aldrich) for 30 minutes at 37°C.
728 The cell suspension was washed twice with PBS. Erythrocytes were removed by
729 hypotonic lysis. Cells were washed twice with PBS and sieved with 30-μm cell strainers
730 (Miltenyi Biotec). The resulting single cells suspension was used to detect leukocyte
731 populations (CD45 BV421 [clone: 104; Biolegend], CD4 PerCPeFluor710 [RM4-5;
732 eBioscience], CD8a APC-Cy7 [53-6.7; Biolegend], CD19 PE-Cy7 [6D5; Biolegend]) and
733 CD4+ Foxp3+ Treg (CD45 BV421, CD4 PerCPeFluor710, Foxp3 PE [FJK-16s; Thermo

734 Fisher]), VDR AlexaFluor647 (D2K6W; Cell Signaling Technologies), Aiolos PE (8B2;
735 Biolegend) and cytokine production by Th-cells (see below).
736
737 Spleens were excised and mononuclear cells were isolated using a syringe plunger and
738 100-µm cell strainers. Red blood cells were removed by hypotonic lysis. Tonicity was
739 restored by the addition of RPMI 1640 (Sigma Aldrich). The resulting cell suspension was
740 washed twice with PBS and used for the isolation of naïve CD4+ T cells according to the
741 manufacturer's instructions (Naive T Cell Isolation Kit II; Miltenyi Biotec). Naive CD4+ T
742 cell purity was assessed by staining for CD4 PerCPeFluor710 (clone: RM4-5), CD44 FITC
743 (IM7), and CD62L PE (mel-14).
744 Naïve T cells were activated with plate bound anti-CD3ε (5 µg/ml, clone: 145-2C11, BD
745 Biosciences) and soluble anti-CD28 (0.5 µg/ml, clone: 37.51, BD Biosciences). Th-subset
746 polarization was induced by exposing naïve CD4+Tcells to following culture conditions
747 for 3 days. Th1 cells: recombinant murine IL-12 (rmIL-12) (10 ng/mL; Peprotech), anti–
748 IL-4 (5 µg/mL; BD Biosciences); Th2 cells: rmIL-4 (20 ng/mL; Peprotech), anti–IFN-γ (5
749 µg/mL; BD Biosciences), and anti–IL-12 (5 µg/mL; BD Biosciences); Treg: rmTGFβ1 (2
750 ng/mL; Peprotech), anti–IL-4 (5 µg/mL), anti–IFN-γ (5 µg/mL) for 3 days. Proliferation of
751 Th1 and Th2 cells was induced using rmIL-2 (20 ng/mL; Peprotech) in the presence of
752 Th-polarizing reagents for an additional 2 days. Polarization efficiency was verified by
753 staining for intracellular cytokines (please see below) or Foxp3 expression (see above).
754
755 For intracellular cytokine staining, cells were stimulated with phorbol 12-myristate 13-
756 acetate (PMA)/ionomycin and brefeldin A (Cell Stimulation Cocktail; Tonbo Biosiences)
757 for 4 hours. Cells were fixed with Fixation Buffer (Biolegend). Cells were permeabilized
758 using 0.3% saponin in FACS buffer (0.5% FBS in PBS). Antibody staining was performed
759 for 30 minutes in the dark using CD4, IFN-γ (XMG1.2-FITC), IL-10 (JES5-16E3-PE), IL-
760 13 (eBio13A-eFluor660), IL-17A (TC11-18H10.1-PE-Cy7). Cells were washed twice with
761 permeabilization buffer and suspended in FACS buffer. For analysis, 30,000 counts (in
762 the CD4+ gate) were recorded on a FACSFortessa (BD Biosciences) and analyzed with
763 FlowJo software (v10; Tree Star).
764

765 *Western blot analyses*

766 Cells were lysed in 50 mmol/L Tris/HCl (pH 7.5), 150 mmol/L NaCl, 1% NP-40, and 1×
767 protease and phosphatase inhibitor mix (both Roche) for 15 minutes on ice. Lysates were
768 clarified, and total protein concentrations were measured with BCA (Pierce). Proteins (20
769 µg) were separated on gradient gels (Mini-PROTEAN® TGX; BioRad) and transferred on
770 a Immun-Blot PVDF membrane (BioRad). Unspecific binding was blocked using 5 % milk
771 powder in TBST for 30 min. Anti-VDR (D2K6W, 1:1000; Cell Signaling Technologies,
772 CST) was incubated in 0.5 % milk powder in TBST overnight at 4° C. Membranes were
773 washed 3 times with TBST and incubated with secondary anti-rabbit IgG, HRP-linked
774 Antibody (#7074; CST) for 2 hours. To control for equal loading, membranes was probed
775 for β-actin (AC-15; 1:10,000; Sigma-Aldrich) expression for 2 hrs. at RT. Protein bands
776 were visualized with Luminol reagent (Pierce) using the ChemiDoc XRS+system
777 (BioRad).

778

779 *Immunofluorescence staining for confocal microscopy*

780 *In vitro* polarized Th2 cells (see above) were stimulated with 100 nm calcitriol (in ethanol)
781 or ethanol [equal v/v] for the final 24 hrs of culture. Cells were washed twice with PBS
782 and spun onto poly-L-lysine coated glass slides. After drying, cells were fixed with 4 %
783 PFA in PBS for 15 min. Cells were permeabilized using 0.2% Triton X-100 in PBS for 20
784 min. Cells were washed 3 times for 5 min with PBS and incubated with Image-iT FX Signal
785 Enhancer (Thermo Fisher Scientific) for 30 min at RT. After three consecutive washes
786 with PBS, unspecific binding was blocked using blocking buffer (PBS/5 % goat serum/0.3
787 % Triton X-100) for 60 min at RT. Primary antibodies directed against CD4-FITC (clone;
788 1:100, BD Biosciences), VDR (D2K6W; 1: 200, CST) were incubated in a humidified
789 chamber over night at 4° C. After 3 washes with PBS, slides were incubated with the
790 secondary reagent, anti-rabbit-Cy3 (1:500; Thermo) for 30 min at RT in the dark. After
791 three more washes with PBS, slides were mounted with ProLong Gold with DAPI
792 according to manufacturer's instructions (Invitrogen). Images were acquired in a single
793 z-plane using a Zeiss immunofluorescence microscope with a 40x objective.

794

795 *Total RNA isolation, quality control, and RNA-sequencing analysis*.

796 Total RNA was isolated using TRIzol™ Reagent (Invitrogen) according to the
797 manufacturer's instructions. Quality was assessed using the Nanodrop 8000
798 spectrophotometer. Sequencing libraries were constructed with the TruSeq® Stranded
799 Total RNA Library Prep Globin Kit (Illumina). Sequencing was performed using a HiSeq.
800 2500 instrument (Illumina). Trimmed reads were mapped to the GRCm38 reference
801 genome using STAR[39]. Read counts were computed with htseq[40]. Data were normalized
802 and differential expression was analyzed with the R package DESeq2 (v.1.34.0) [43] using
803 a false discovery rate (FDR) < 0.05.
804
805 *Pathway enrichment, Overrepresentation and Gene Set Enrichment analysis*.
806 KEGG pathway, overrepresentation and gene set enrichment analyses were performed
807 with the "enrichKEGG", "enrichr" and "GSEA" function in the R package "clusterProfiler"
808 (v.3.10.1) with default settings [44]. P-values were adjusted using the BH-FDR correction
809 and enriched terms with a p-adj.<0.05 selected.
810
811 *Network analysis*
812 RNA-Sequencing data extracted from murine Th2 cells were analyzed using the R
813 package DESeq2 (v.1.22.2) [43]. Raw counts were normalized and transformed for variance
814 stabilization using the DESeq2 function rlog (regularized-logarithm transformation). Batch
815 effects were removed using the function removeBatchEffect of the R package LIMMA[45].
816 Gene with counts lower than 5 in at least one sample were removed for downstream
817 analyses.
818
819 Differential expression analysis was performed between control Th2 cells versus calcitriol
820 stimulated Th2 cells using DeSeq2 [43]. The design matrix was built to consider batch
821 effects derived from the RNA isolation process. DESeq2-independent filtering was
822 applied [43] and P values were corrected for multiple hypothesis testing by using the
823 Benjamini-Hochberg (BH)-FDR adjustment [46].
824
825 The PPI network used in our network analysis was developed by Silverbush et al. [17]. As
826 described in the original paper, this human PPI network was reconstructed by integrating

827 large scale PPI databases, drug response repositories, and cancer genomics data. Only
828 the largest connected component of the network was considered, resulting in an
829 interactome of 15,500 proteins and 234,585 consensus-oriented interactions. Conversion
830 between murine and human gene IDs was performed using the BioMart conversion tool
831 [47]. We also assumed a one-to-one correspondence between genes and their protein
832 products in the entire analysis.
833
834 To identify the active signaling paths in control and calcitriol stimulated Th2 cells, we
835 modelled the transmission of the molecular signal as a sequential path on the PPI network
836 (called a network path) that starts from a receptor, connects the receptor to multiple
837 intermediate proteins, and leads to a transcription factor. Receptors and transcription
838 factors were selected from a predefined list based on their role in Th2 cell biology and IL-
839 2 expression (Extended Data Table 8). CD3, CD28, IL-4R, IL-13R were selected based
840 on their role in Th2 differentiation. The IL-2R complex was included due to being a target
841 of vitamin D signaling. TGFβRs were selected based on the immunomodulatory activity
842 of this signaling path in CD4+ T cells. role in mediating immunoregulation. Using this
843 subset of receptors and transcription factors as input for the implementation of our
844 network analysis, we computed all the shortest paths connecting each receptor-
845 transcription factor pair on the PPI network. For both control and calcitriol stimulated Th2
846 cells, we ranked each network path based on the average expression of the path's nodes.
847 The top selected paths represent the most active downstream processes in Th2 cells in
848 each condition.
849
850 *mRNA isolation, reverse transcription, and real-time RT-PCR.*
851 Total RNA from in vitro polarized Th2 cells was isolated with the RNeasy Mini Kit
852 (Qiagen). First-strand cDNA synthesis was performed with the Omniscript kit (Qiagen).
853 Quantitative real-time PCR was performed with the SsoFast EvaGreen Supermix Kit
854 (BioRad) on a AriaMx Real-time PCR System (Agilent) as per manufacturer's instructions.
855 Primers sequences used in this study are listed in Extended Data Table 9. Relative gene
856 expression levels were calculated with the $2^{-\Delta\Delta Ct}$ method, with normalization to the murine
857 ribosomal L32 as the housekeeping gene. Data are presented as fold induction over the

respective control groups (vehicle or WT). All standard procedures were performed according to the manufacturer's instructions.

Quantification and statistical analysis.

For each figure the number of replicates per experiment is indicated in the corresponding figure legend. In the figures, mean and standard error of the mean (s.e.m.) are presented and error bars represent the mean ± s.e.m. Two group comparisons were analyzed using unpaired two-tailed Student's t-tests (parametric data) and Mann–Whitney U-test (non-parametric data). Multiple group comparisons were analyzed with Kruskal-Wallis and One-way ANOVA test with Tukey's post hoc analysis. *In vivo* experiments were analyzed using Mixed-effect analysis or Two-way ANOVA test with Holm-Šidák's post-hoc analysis (factors: genotype & exposure, diet & exposure). Prism 9.2 (GraphPad Software) was used to calculate statistics. P values of less than 0.05 were considered statistically significant.

Acknowledgements: We wish to thank the VDAART trial participants and clinical staff for their critical work on the VDAART study. We wish to thank our Channing colleagues for comments, the National Heart Lung and Blood institute for funding via 5P01HL132825, 5UH3OD023268 and 5K25HL150336, and the German Society for Clinical Chemistry and Laboratory Medicine (DGKL) and the German Research Foundation (DFG) for funding via KI 1868/3-1.

Author information: These authors jointly supervised this work: Ayşe Kılıç, Scott T. Weiss

Contributions

A.K. and S.T.W. designed the experiments, analyzed data, and wrote the manuscript. A.K., M.G.D., T.R.B., J.R.Q., A.O.S, J.K., T.N., H.Y.P., N.K. and R.E.A performed experiments. A.H., E.M., M.D.M. and R. C. analyzed data. M.D. and K.G. provided critical mouse lines and scientific input. A.A.L. assisted on VDAART related analyses. H.R. and

B.D.L. supervised experiments and provided critical scientific input. All authors critically reviewed the manuscript.

Ethics declarations: none

Competing interest

Dr. Weiss receives royalties from UpToDate and is an investor in Histolix. All other authors declare no competing interests.

Supplementary Information is available for this paper.

Correspondence and requests for materials should be addressed to Ayşe Kılıç and Scott T. Weiss

Peer review information

Reprints and permissions information is available at www.nature.com/reprints.

References

1. Litonjua, A. A. & Weiss, S. T. Is vitamin D deficiency to blame for the asthma epidemic? *The Journal of allergy and clinical immunology* **120,** 1031–1035; 10.1016/j.jaci.2007.08.028 (2007).
2. Bouzigon, E. *et al.* Effect of 17q21 variants and smoking exposure in early-onset asthma. *The New England journal of medicine* **359,** 1985–1994; 10.1056/NEJMoa0806604 (2008).
3. Kelly, R. S. *et al.* The role of the 17q21 genotype in the prevention of early childhood asthma and recurrent wheeze by vitamin D. *The European respiratory journal* **54**; 10.1183/13993003.00761-2019 (2019).
4. Schmiedel, B. J. *et al.* 17q21 asthma-risk variants switch CTCF binding and regulate IL-2 production by T cells. *Nature communications* **7,** 13426; 10.1038/ncomms13426 (2016).
5. Moffatt, M. F. *et al.* Genetic variants regulating ORMDL3 expression contribute to the risk of childhood asthma. *Nature* **448,** 470–473; 10.1038/nature06014 (2007).
6. Litherland, S. A. *et al.* Signal transduction activator of transcription 5 (STAT5) dysfunction in autoimmune monocytes and macrophages. *Journal of autoimmunity* **24,** 297–310; 10.1016/j.jaut.2005.02.001 (2005).
7. Kara, S., Pirela-Morillo, G. A., Gilliam, C. T. & Wilson, G. D. Identification of novel susceptibility genes associated with seven autoimmune disorders using whole genome

molecular interaction networks. *Journal of autoimmunity* **97,** 48–58; 10.1016/j.jaut.2018.10.002 (2019).

8. Buniello, A. *et al.* The NHGRI-EBI GWAS Catalog of published genome-wide association studies, targeted arrays and summary statistics 2019. *Nucleic acids research* **47,** D1005-D1012; 10.1093/nar/gky1120 (2019).
9. Syreeni, A. *et al.* Genome-wide search for genes affecting the age at diagnosis of type 1 diabetes. *Journal of internal medicine* **289,** 662–674; 10.1111/joim.13187 (2021).
10. Shrine, N. *et al.* Moderate-to-severe asthma in individuals of European ancestry: a genome-wide association study. *The Lancet. Respiratory medicine* **7,** 20–34; 10.1016/S2213-2600(18)30389-8 (2019).
11. Marinho, S., Custovic, A., Marsden, P., Smith, J. A. & Simpson, A. 17q12-21 variants are associated with asthma and interact with active smoking in an adult population from the United Kingdom. *Annals of allergy, asthma & immunology : official publication of the American College of Allergy, Asthma, & Immunology* **108,** 402-411.e9; 10.1016/j.anai.2012.03.002 (2012).
12. Hitomi, Y. *et al.* Identification of the functional variant driving ORMDL3 and GSDMB expression in human chromosome 17q12-21 in primary biliary cholangitis. *Scientific reports* **7,** 2904; 10.1038/s41598-017-03067-3 (2017).
13. Keshari, P. K. *et al.* Allelic imbalance of multiple sclerosis susceptibility genes IKZF3 and IQGAP1 in human peripheral blood. *BMC genetics* **17,** 59; 10.1186/s12863-016-0367-4 (2016).
14. Verlaan, D. J. *et al.* Allele-specific chromatin remodeling in the ZPBP2/GSDMB/ORMDL3 locus associated with the risk of asthma and autoimmune disease. *American journal of human genetics* **85,** 377–393; 10.1016/j.ajhg.2009.08.007 (2009).
15. Devereux, G. *et al.* Maternal vitamin D intake during pregnancy and early childhood wheezing. *The American journal of clinical nutrition* **85,** 853–859; 10.1093/ajcn/85.3.853 (2007).
16. Sakai, Y., Kishimoto, J. & Demay, M. B. Metabolic and cellular analysis of alopecia in vitamin D receptor knockout mice. *The Journal of clinical investigation* **107,** 961–966; 10.1172/JCI11676 (2001).
17. Silverbush, D. & Sharan, R. A systematic approach to orient the human protein-protein interaction network. *Nature communications* **10,** 3015; 10.1038/s41467-019-10887-6 (2019).
18. Quintana, F. J. *et al.* Aiolos promotes TH17 differentiation by directly silencing Il2 expression. *Nature immunology* **13,** 770–777; 10.1038/ni.2363 (2012).
19. Raby, B. A. *et al.* Association of vitamin D receptor gene polymorphisms with childhood and adult asthma. *American journal of respiratory and critical care medicine* **170,** 1057–1065; 10.1164/rccm.200404-447OC (2004).
20. Camargo, C. A. *et al.* Maternal intake of vitamin D during pregnancy and risk of recurrent wheeze in children at 3 y of age. *The American journal of clinical nutrition* **85,** 788–795; 10.1093/ajcn/85.3.788 (2007).
21. van der Pligt, P. *et al.* Associations of Maternal Vitamin D Deficiency with Pregnancy and Neonatal Complications in Developing Countries: A Systematic Review. *Nutrients* **10**; 10.3390/nu10050640 (2018).
22. Roth, D. E. *et al.* Global prevalence and disease burden of vitamin D deficiency: a roadmap for action in low- and middle-income countries. *Annals of the New York Academy of Sciences* **1430,** 44–79; 10.1111/nyas.13968 (2018).

968 23. Cashman, K. D. Vitamin D Deficiency: Defining, Prevalence, Causes, and Strategies of
969 Addressing. *Calcified tissue international* **106,** 14–29; 10.1007/s00223-019-00559-4 (2020).
970 24. Litonjua, A. A. *et al.* The Vitamin D Antenatal Asthma Reduction Trial (VDAART):
971 rationale, design, and methods of a randomized, controlled trial of vitamin D supplementation
972 in pregnancy for the primary prevention of asthma and allergies in children. *Contemporary*
973 *clinical trials* **38,** 37–50; 10.1016/j.cct.2014.02.006 (2014).
974 25. Litonjua, A. A. *et al.* Effect of Prenatal Supplementation With Vitamin D on Asthma or
975 Recurrent Wheezing in Offspring by Age 3 Years: The VDAART Randomized Clinical Trial.
976 *JAMA* **315,** 362–370; 10.1001/jama.2015.18589 (2016).
977 26. Litonjua, A. A. *et al.* Six-Year Follow-up of a Trial of Antenatal Vitamin D for Asthma
978 Reduction. *The New England journal of medicine* **382,** 525–533; 10.1056/NEJMoa1906137
979 (2020).
980 27. Wolsk, H. M. *et al.* Prenatal vitamin D supplementation reduces risk of asthma/recurrent
981 wheeze in early childhood: A combined analysis of two randomized controlled trials. *PloS*
982 *one* **12,** e0186657; 10.1371/journal.pone.0186657 (2017).
983 28. Wolsk, H. M. *et al.* Vitamin D supplementation in pregnancy, prenatal 25(OH)D levels, race,
984 and subsequent asthma or recurrent wheeze in offspring: Secondary analyses from the
985 Vitamin D Antenatal Asthma Reduction Trial. *The Journal of allergy and clinical*
986 *immunology* **140,** 1423-1429.e5; 10.1016/j.jaci.2017.01.013 (2017).
987 29. Miller, M. *et al.* ORMDL3 transgenic mice have increased airway remodeling and airway
988 responsiveness characteristic of asthma. *Journal of immunology (Baltimore, Md. : 1950)* **192,**
989 3475–3487; 10.4049/jimmunol.1303047 (2014).
990 30. Zhang, Y. *et al.* The ORMDL3 Asthma Gene Regulates ICAM1 and Has Multiple Effects on
991 Cellular Inflammation. *American journal of respiratory and critical care medicine* **199,** 478–
992 488; 10.1164/rccm.201803-0438OC (2019).
993 31. Pfeffer, P. E. & Hawrylowicz, C. M. Vitamin D in Asthma: Mechanisms of Action and
994 Considerations for Clinical Trials. *Chest* **153,** 1229–1239; 10.1016/j.chest.2017.09.005
995 (2018).
996 32. Baeke, F. *et al.* Human T lymphocytes are direct targets of 1,25-dihydroxyvitamin D3 in the
997 immune system. *The Journal of steroid biochemistry and molecular biology* **121,** 221–227;
998 10.1016/j.jsbmb.2010.03.037 (2010).
999 33. Zhu, J., Cote-Sierra, J., Guo, L. & Paul, W. E. Stat5 activation plays a critical role in Th2
1000 differentiation. *Immunity* **19,** 739–748; 10.1016/s1074-7613(03)00292-9 (2003).
1001 34. Fishilevich, S. *et al.* GeneHancer: genome-wide integration of enhancers and target genes in
1002 GeneCards. *Database : the journal of biological databases and curation* **2017**;
1003 10.1093/database/bax028 (2017).
1004 35. Neme, A., Seuter, S. & Carlberg, C. Vitamin D-dependent chromatin association of CTCF in
1005 human monocytes. *Biochimica et biophysica acta* **1859,** 1380–1388;
1006 10.1016/j.bbagrm.2016.08.008 (2016).
1007 36. Neme, A., Seuter, S. & Carlberg, C. Selective regulation of biological processes by vitamin D
1008 based on the spatio-temporal cistrome of its receptor. *Biochimica et biophysica acta. Gene*
1009 *regulatory mechanisms* **1860,** 952–961; 10.1016/j.bbagrm.2017.07.002 (2017).
1010 37. Ramagopalan, S. V. *et al.* A ChIP-seq defined genome-wide map of vitamin D receptor
1011 binding: associations with disease and evolution. *Genome research* **20,** 1352–1360;
1012 10.1101/gr.107920.110 (2010).

1013 38. Lu, X. *et al.* MTA2/NuRD Regulates B Cell Development and Cooperates with OCA-B in
1014 Controlling the Pre-B to Immature B Cell Transition. *Cell reports* **28,** 472-485.e5;
1015 10.1016/j.celrep.2019.06.029 (2019).
1016 39. Dobin, A. *et al.* STAR: ultrafast universal RNA-seq aligner. *Bioinformatics (Oxford,*
1017 *England)* **29,** 15–21; 10.1093/bioinformatics/bts635 (2013).
1018 40. Anders, S., Pyl, P. T. & Huber, W. HTSeq--a Python framework to work with high-
1019 throughput sequencing data. *Bioinformatics (Oxford, England)* **31,** 166–169;
1020 10.1093/bioinformatics/btu638 (2015).
1021 41. McCarthy, D. J., Chen, Y. & Smyth, G. K. Differential expression analysis of multifactor
1022 RNA-Seq experiments with respect to biological variation. *Nucleic acids research* **40,** 4288–
1023 4297; 10.1093/nar/gks042 (2012).
1024 42. Li, Y. C. *et al.* Normalization of mineral ion homeostasis by dietary means prevents
1025 hyperparathyroidism, rickets, and osteomalacia, but not alopecia in vitamin D receptor-
1026 ablated mice. *Endocrinology* **139,** 4391–4396; 10.1210/endo.139.10.6262 (1998).
1027 43. Love, M. I., Huber, W. & Anders, S. Moderated estimation of fold change and dispersion for
1028 RNA-seq data with DESeq2. *Genome biology* **15,** 550; 10.1186/s13059-014-0550-8 (2014).
1029 44. Yu, G., Wang, L.-G., Han, Y. & He, Q.-Y. clusterProfiler: an R package for comparing
1030 biological themes among gene clusters. *Omics : a journal of integrative biology* **16,** 284–287;
1031 10.1089/omi.2011.0118 (2012).
1032 45. Ritchie, M. E. *et al.* limma powers differential expression analyses for RNA-sequencing and
1033 microarray studies. *Nucleic acids research* **43,** e47; 10.1093/nar/gkv007 (2015).
1034 46. Benjamini, Y., Drai, D., Elmer, G., Kafkafi, N. & Golani, I. Controlling the false discovery
1035 rate in behavior genetics research. *Behavioural brain research* **125,** 279–284; 10.1016/s0166-
1036 4328(01)00297-2 (2001).
1037 47. Smedley, D. *et al.* The BioMart community portal: an innovative alternative to large,
1038 centralized data repositories. *Nucleic acids research* **43,** W589-98; 10.1093/nar/gkv350
1039 (2015).
1040

a
Th1 diseases
Th2 diseases
SNPs with p ≤ 10^−6
b
Chromosome Band
Common dbSNP(153)
UCSC Genes (RefSeq, GenBank, CCDS, Rfam, tRNAs & Comparative Genomics)
VDR (LCL)
VDR (THP-1)
VDR-CTCF (THP-1)
CTCF (THP-1)
IKZF3 (697)
Transcription Factor ChIP-seq Peaks (338 factors in 130 cell types) from ENCODE 3
Layered H3K27Ac
H3K27Ac Mark (Often Found Near Active Regulatory Elements) on 7 cell lines from ENCODE
Interactions between GeneHancer regulatory elements and genes (Double Elite)
c
D'
1.0
0.0
SNPs in 17q12-21.1
SNPs in 17q21.2
Th1 disease-associated SNPs
Th2 diseases-associated SNPs
VDR binding site SNPs
Functional asthma SNPs from the literature
rs2941522
rs12946510
rs35564481
rs1453559
rs12936231
rs4065275
rs111708606
rs62078362
rs4793244

Figure 1

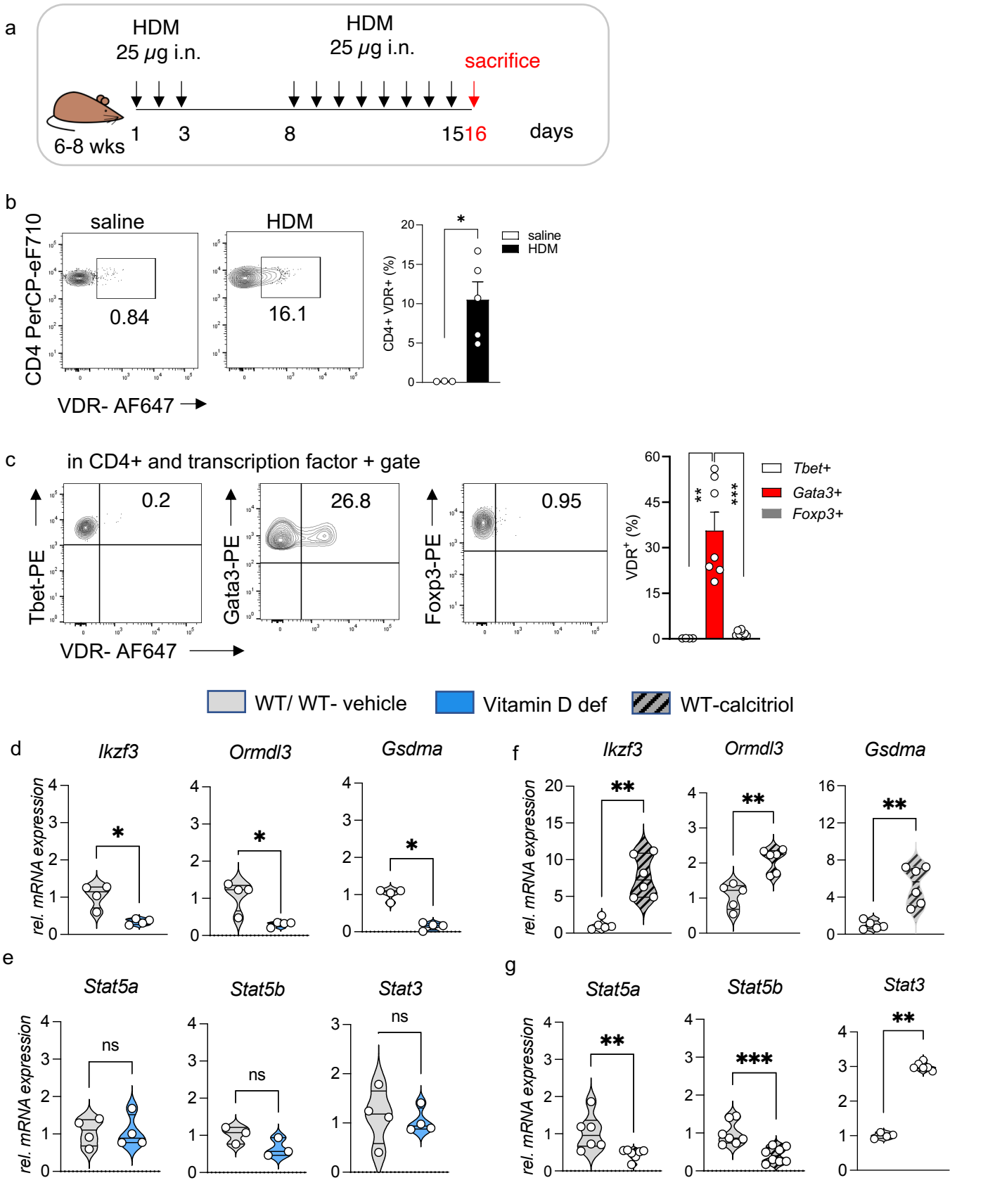
a
HDM
25 μg i.n.
HDM
25 μg i.n.
sacrifice
6-8 wks
1
3
8
15
16
days
b
saline
HDM
CD4 PerCP-eF710
0.84
16.1
VDR- AF647
CD4+ VDR+ (%)
saline
HDM
c
in CD4+ and transcription factor + gate
Tbet-PE
Gata3-PE
Foxp3-PE
0.2
26.8
0.95
VDR- AF647
VDR+ (%)
Tbet+
Gata3+
Foxp3+
WT/ WT- vehicle
Vitamin D def
WT-calcitriol
d
Ikzf3
Ormdl3
Gsdma
rel. mRNA expression
f
Ikzf3
Ormdl3
Gsdma
rel. mRNA expression
e
Stat5a
Stat5b
Stat3
rel. mRNA expression
ns
g
Stat5a
Stat5b
Stat3
rel. mRNA expression

Figure 2

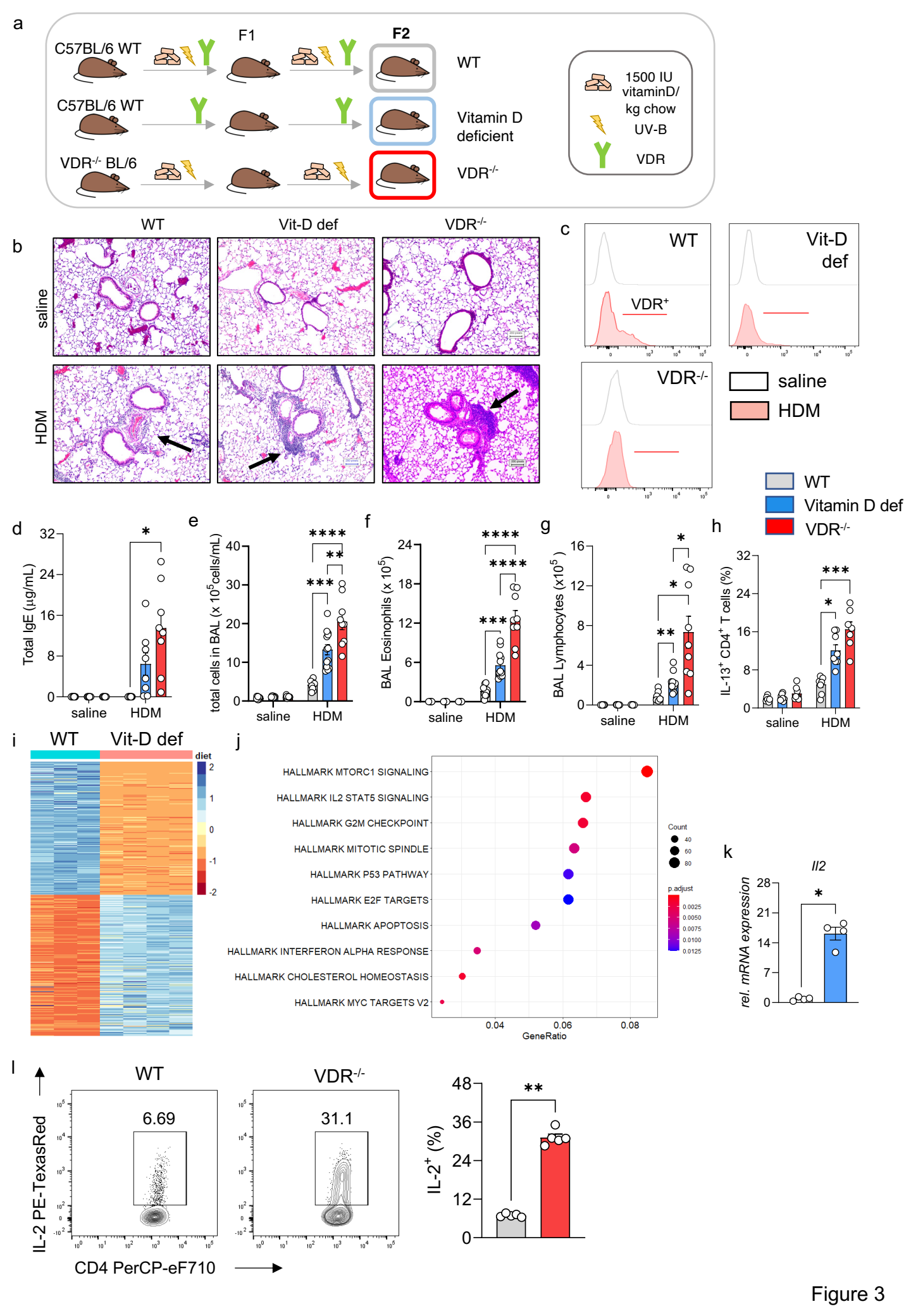
a
C57BL/6 WT
F1
F2
WT
C57BL/6 WT
Vitamin D deficient
VDR-/- BL/6
VDR-/-
1500 IU vitaminD/ kg chow
UV-B
VDR
b
WT
Vit-D def
VDR-/-
saline
HDM
c
WT
Vit-D def
VDR+
VDR-/-
saline
HDM
WT
Vitamin D def
VDR-/-
d
Total IgE (µg/mL)
saline
HDM
e
total cells in BAL (x 10^5 cells/mL)
saline
HDM
f
BAL Eosinophils (x 10^5)
saline
HDM
g
BAL Lymphocytes (x10^5)
saline
HDM
h
IL-13+ CD4+ T cells (%)
saline
HDM
i
WT
Vit-D def
diet
j
HALLMARK MTORC1 SIGNALING
HALLMARK IL2 STAT5 SIGNALING
HALLMARK G2M CHECKPOINT
HALLMARK MITOTIC SPINDLE
HALLMARK P53 PATHWAY
HALLMARK E2F TARGETS
HALLMARK APOPTOSIS
HALLMARK INTERFERON ALPHA RESPONSE
HALLMARK CHOLESTEROL HOMEOSTASIS
HALLMARK MYC TARGETS V2
GeneRatio
Count
p.adjust
k
Il2
rel. mRNA expression
l
WT
VDR-/-
6.69
31.1
IL-2 PE-TexasRed
CD4 PerCP-eF710
IL-2+ (%)

Figure 3

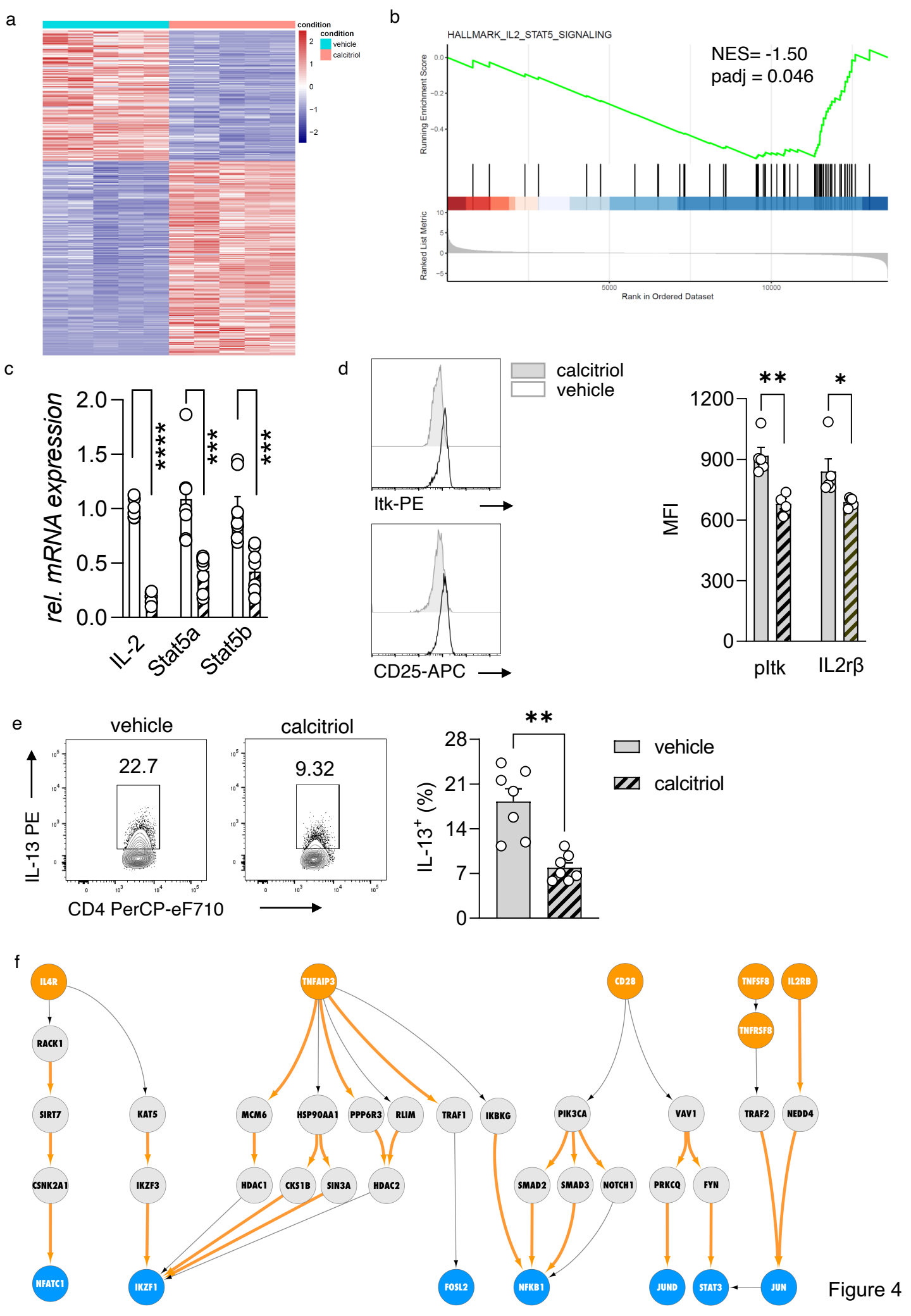
a
condition
condition
vehicle
calcitriol
2
1
0
−1
−2
b
HALLMARK_IL2_STAT5_SIGNALING
NES= -1.50
padj = 0.046
Running Enrichment Score
0.0
−0.2
−0.4
Ranked List Metric
10
5
0
−5
5000
10000
Rank in Ordered Dataset
c
rel. mRNA expression
2.0
1.5
1.0
0.5
0.0
****
***
***
IL-2
Stat5a
Stat5b
d
calcitriol
vehicle
Itk-PE
CD25-APC
**
*
1200
900
600
300
0
MFI
pItk
IL2rβ
e
vehicle
calcitriol
22.7
9.32
IL-13 PE
CD4 PerCP-eF710
**
28
21
14
7
0
IL-13+ (%)
vehicle
calcitriol
f
IL4R
TNFAIP3
CD28
TNFSF8
IL2RB
TNFRSF8
RACK1
SIRT7
KAT5
MCM6
HSP90AA1
PPP6R3
RLIM
TRAF1
IKBKG
PIK3CA
VAV1
TRAF2
NEDD4
CSNK2A1
IKZF3
HDAC1
CKS1B
SIN3A
HDAC2
SMAD2
SMAD3
NOTCH1
PRKCQ
FYN
NFATC1
IKZF1
FOSL2
NFKB1
JUND
STAT3
JUN

Figure 4

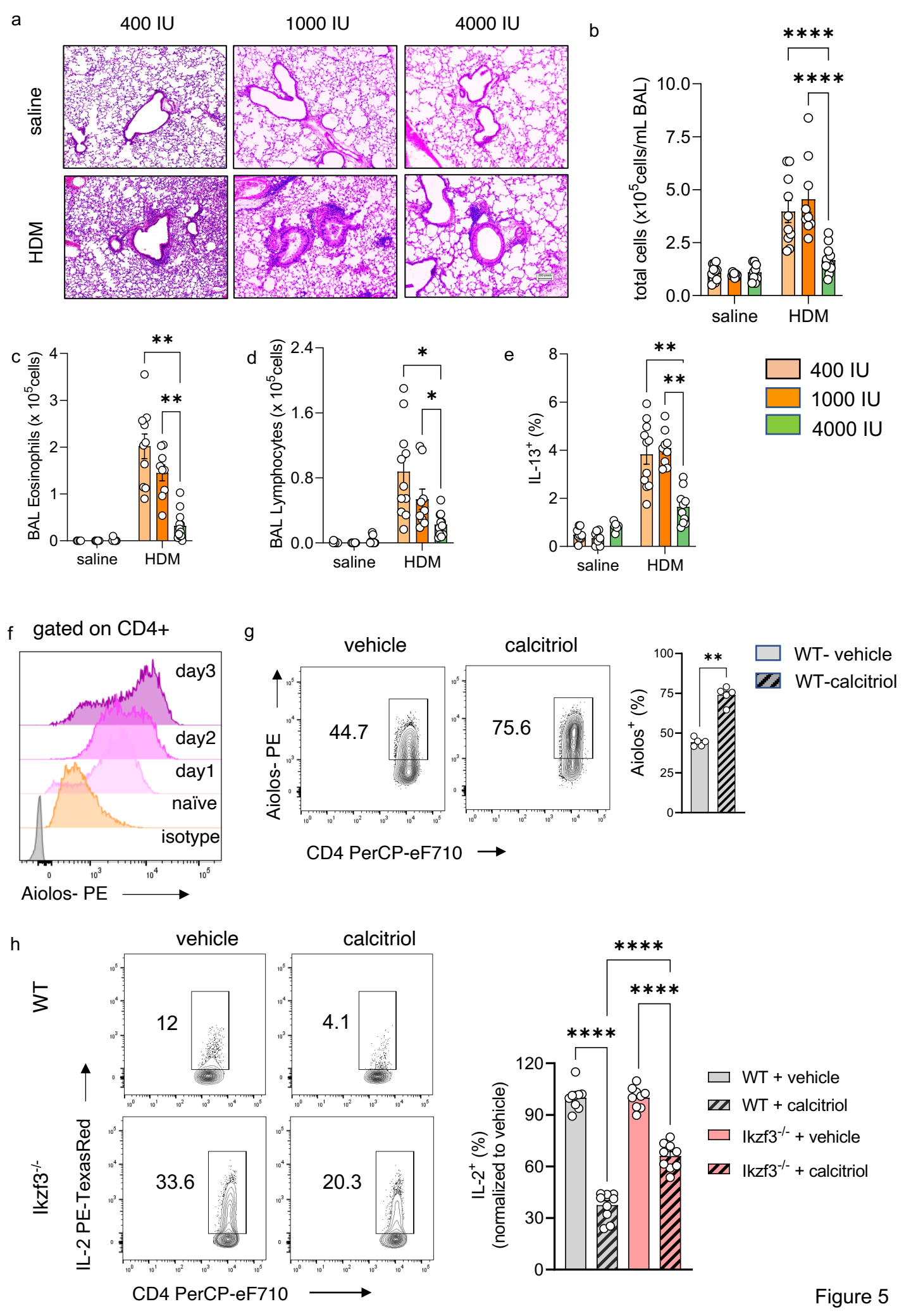
a
400 IU
1000 IU
4000 IU
saline
HDM
b
total cells (x10^5 cells/mL BAL)
10.0
7.5
5.0
2.5
0.0
saline
HDM
****
****
c
BAL Eosinophils (x 10^5 cells)
4
3
2
1
0
saline
HDM
**
**
d
BAL Lymphocytes (x 10^5 cells)
2.4
1.6
0.8
0.0
saline
HDM
*
*
e
IL-13+ (%)
8
6
4
2
0
saline
HDM
**
**
400 IU
1000 IU
4000 IU
f
gated on CD4+
day3
day2
day1
naïve
isotype
Aiolos- PE
g
vehicle
calcitriol
44.7
75.6
Aiolos- PE
CD4 PerCP-eF710
Aiolos+ (%)
100
75
50
25
0
**
WT- vehicle
WT-calcitriol
h
vehicle
calcitriol
WT
Ikzf3-/-
12
4.1
33.6
20.3
IL-2 PE-TexasRed
CD4 PerCP-eF710
IL-2+ (%)
(normalized to vehicle)
120
90
60
30
0
****
****
****
WT + vehicle
WT + calcitriol
Ikzf3-/- + vehicle
Ikzf3-/- + calcitriol

Figure 5

a

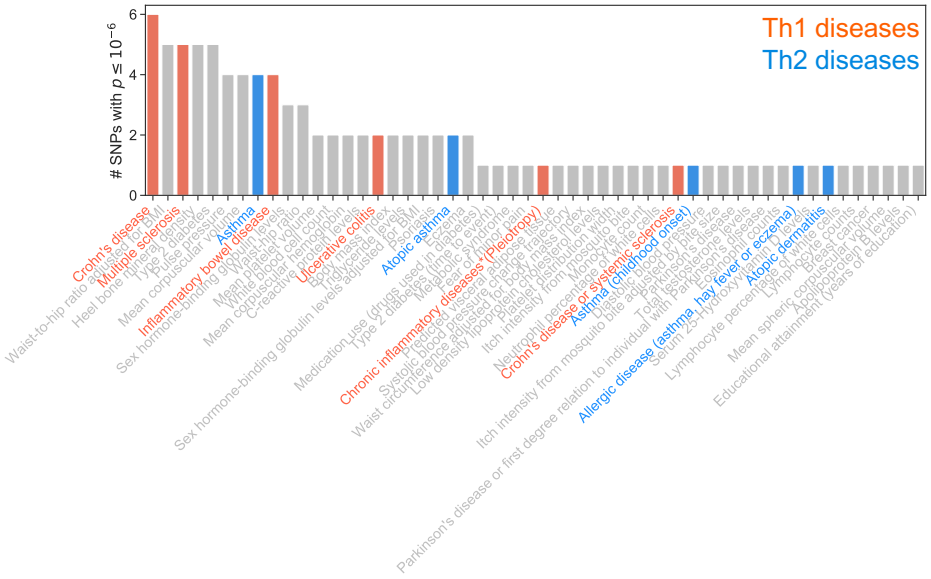

b

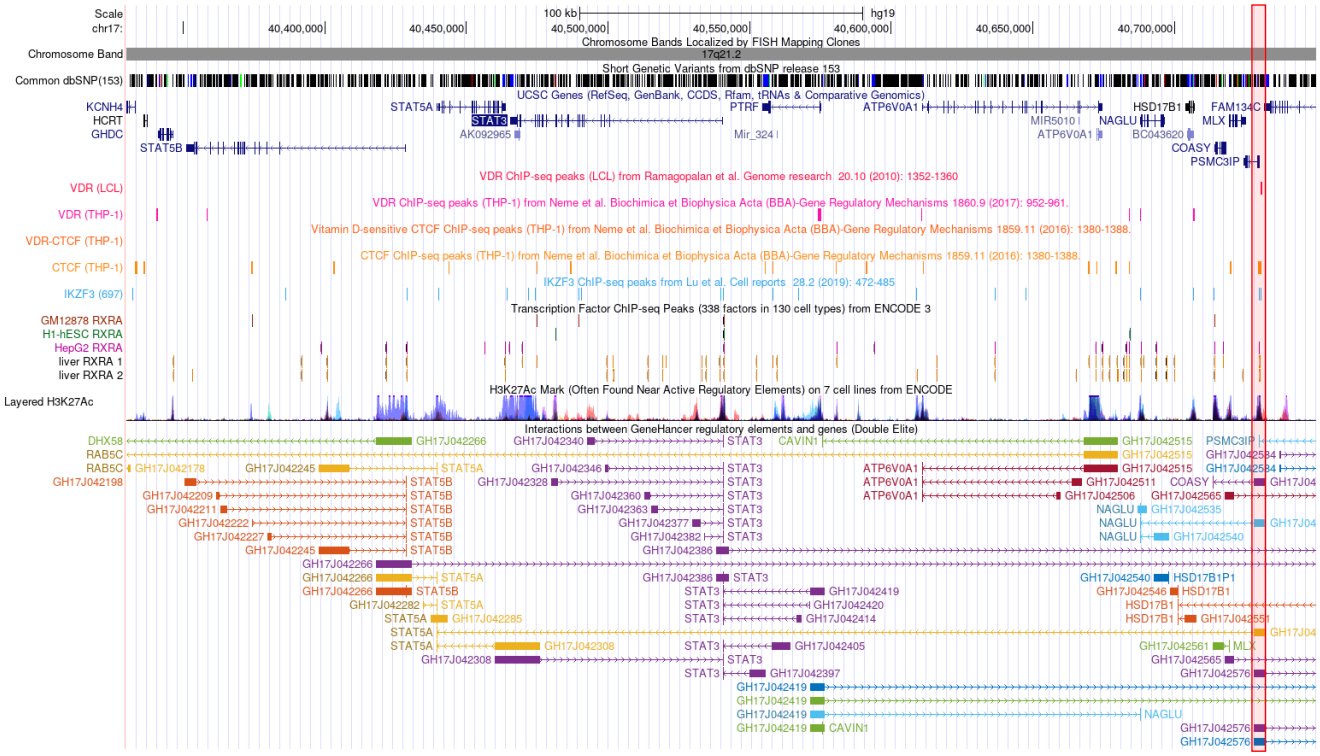

Extended Data Figure 1

a gating strategy

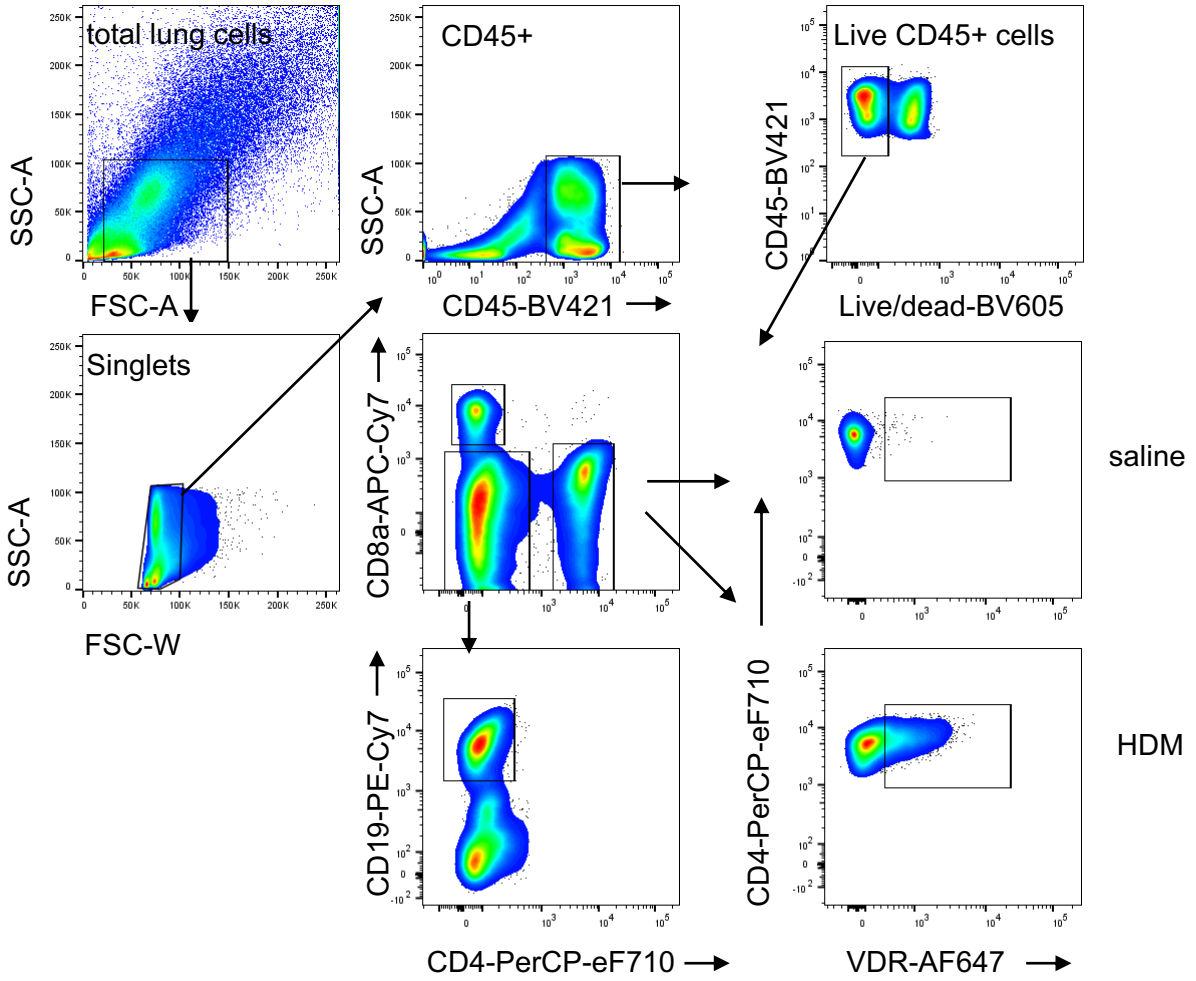

b

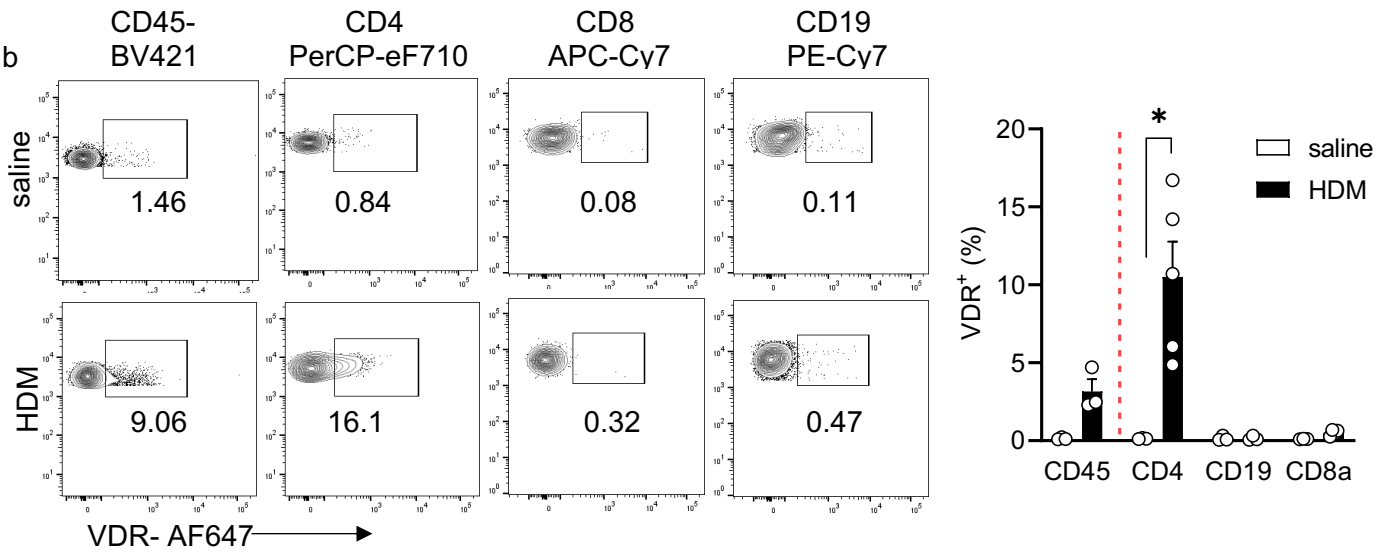

c gated on CD45+ CD4+

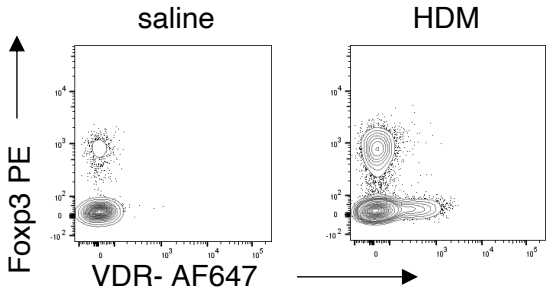

Extended Data Figure 2

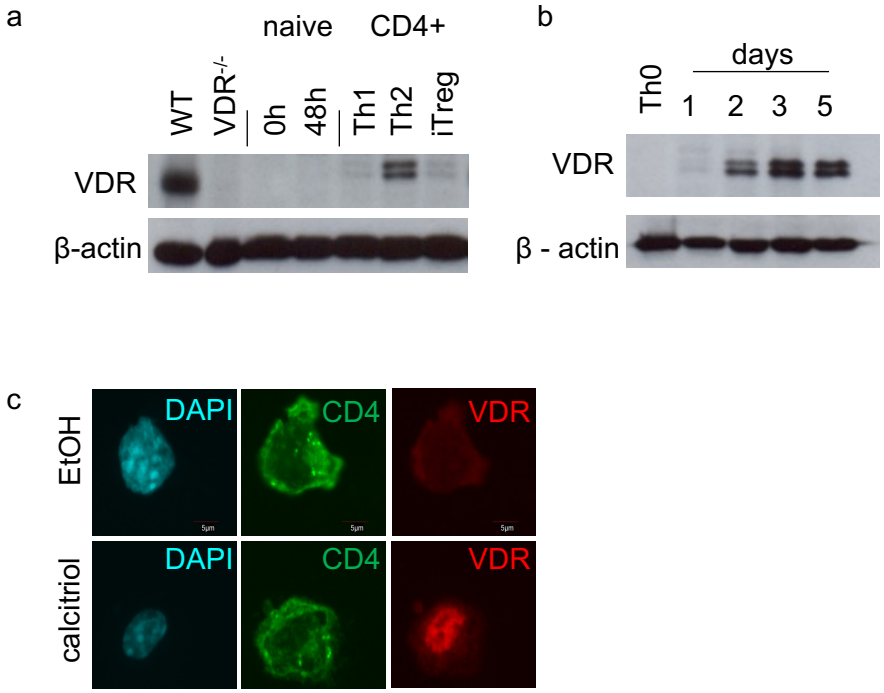

Extended Data Figure 3

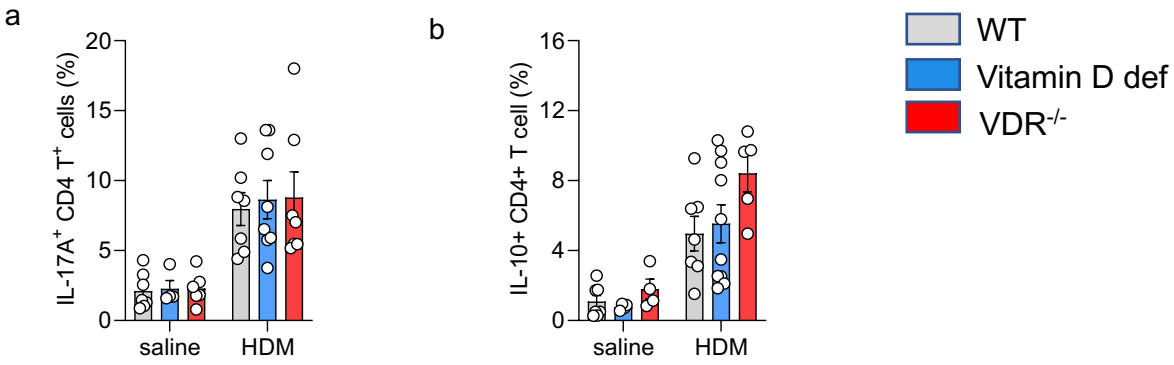

Extended Data Figure 4

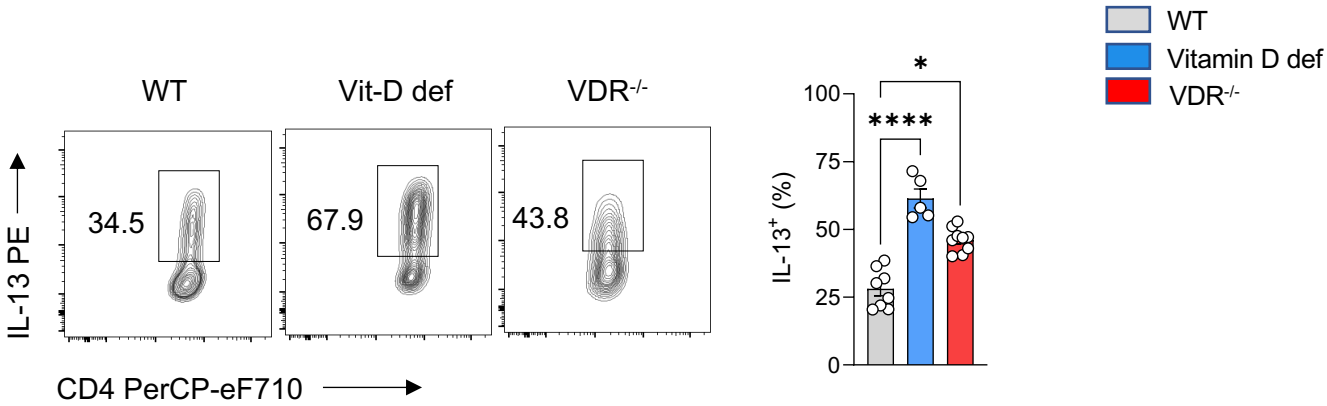

Extended Data Figure 5

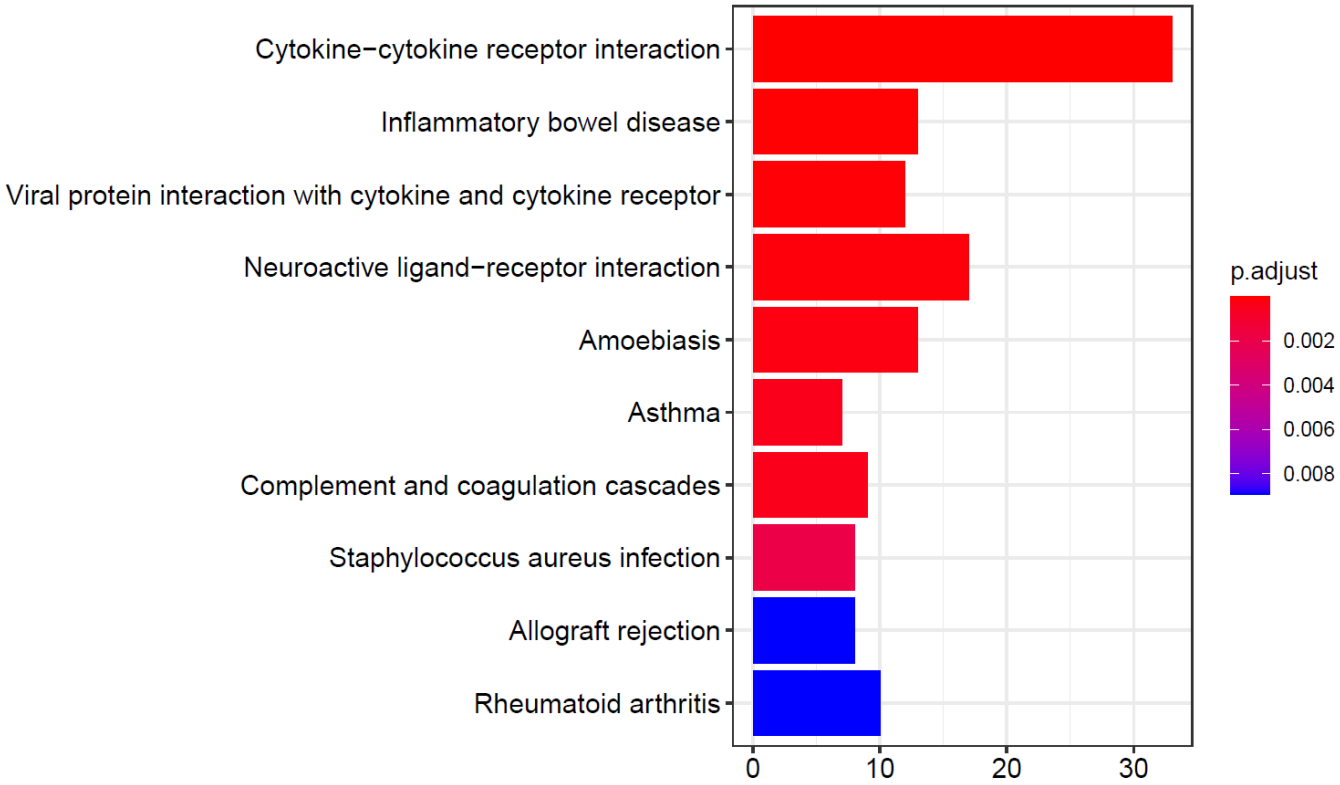

Extended Data Figure 6

a

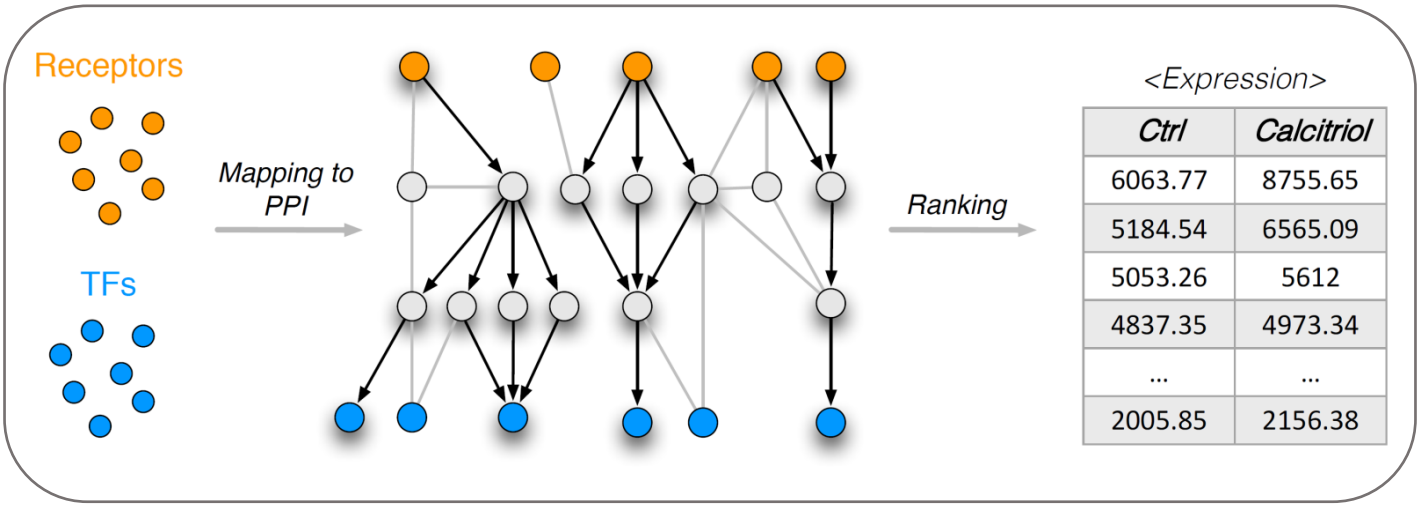

b

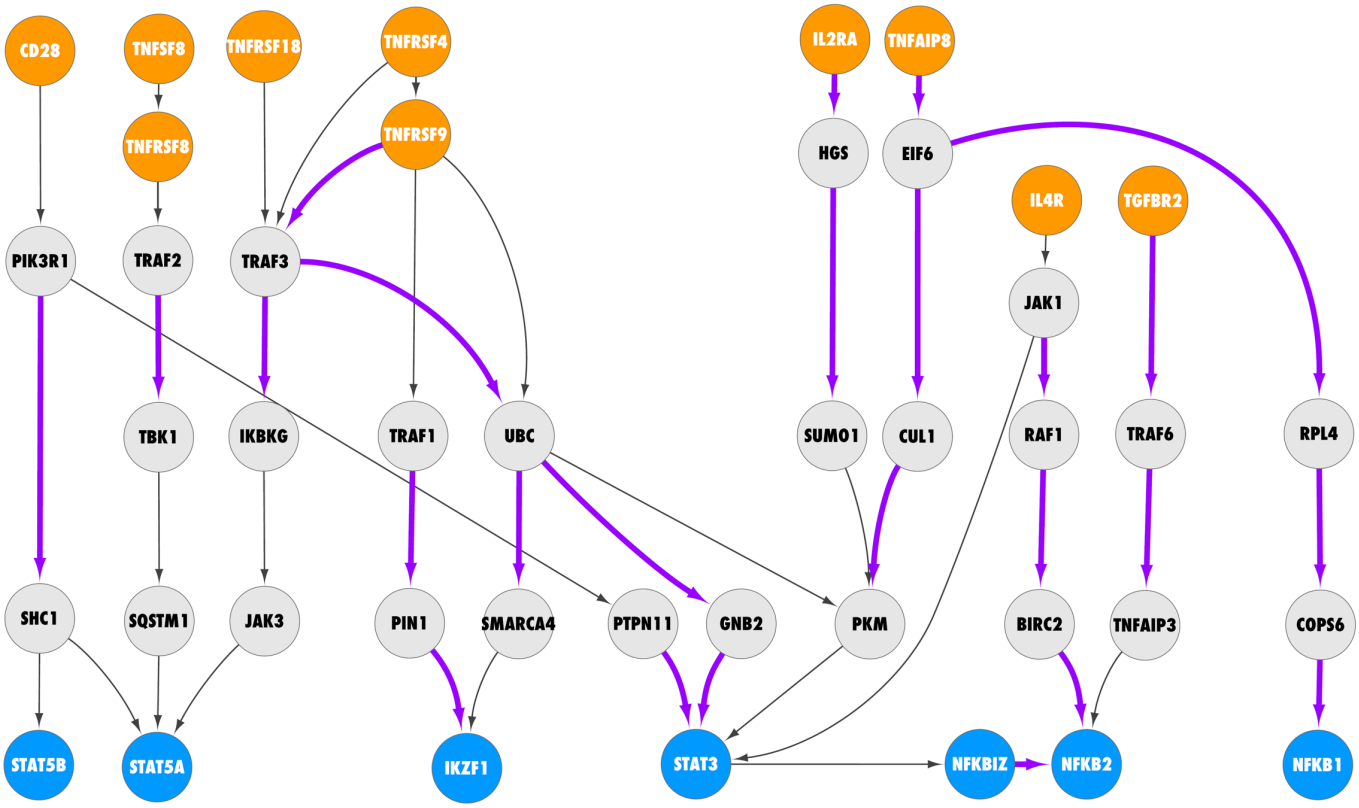

Extended Data Figure 7

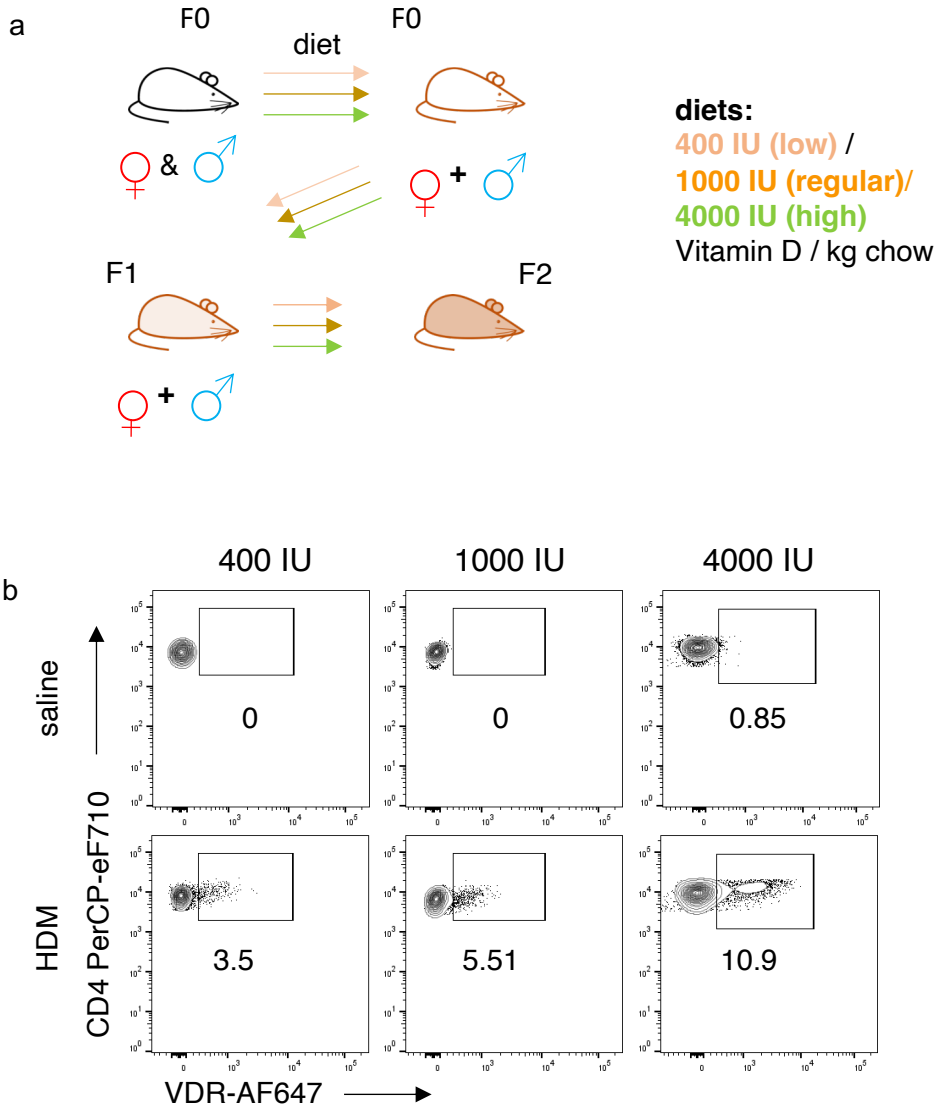

Extended Data Figure 8

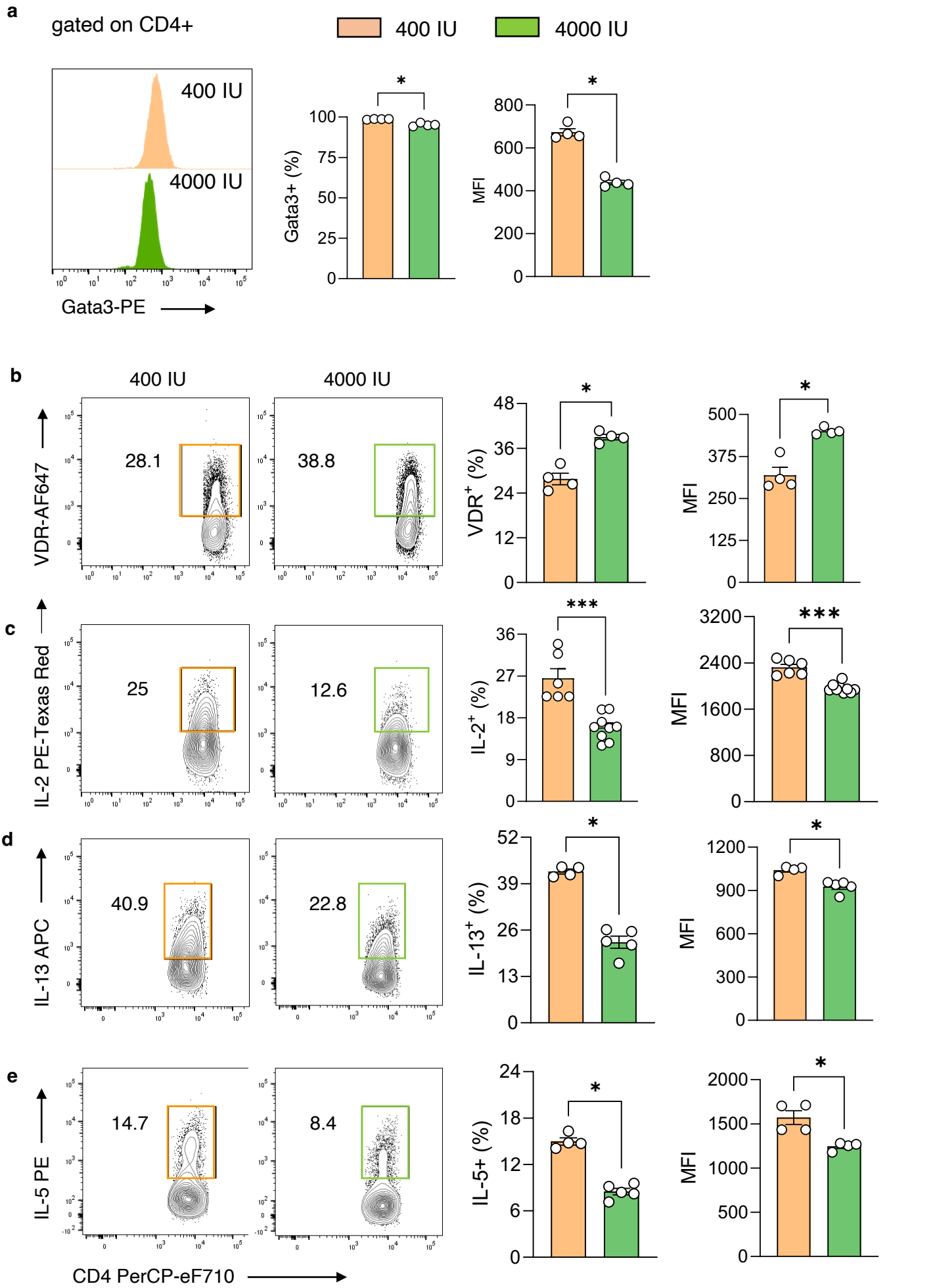

Extended Data Figure 9

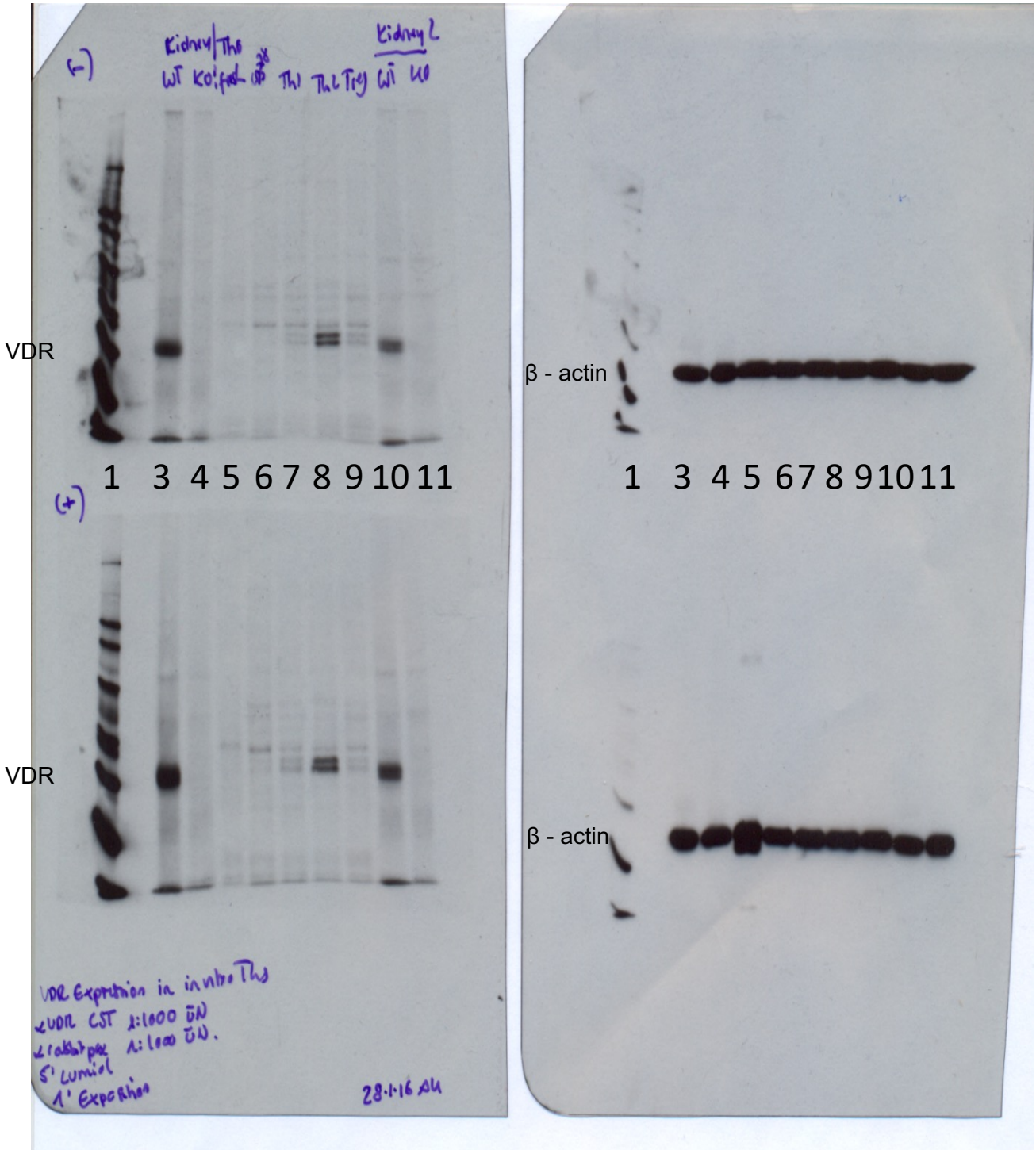

Loading order:
1- marker
2- empty
3- WT kidney sample: positive control
4- VDR-/- kidney sample: negative control
5- CD4+ CD62L+CD44- naïve T cells fresh
6- Th0 cells (24 h CD3 & CD28 stimulation)
7- in vitro Th1
8- in vitro Th2
9- in vitro iTreg
10- WT kidney sample: positive control
11- VDR-/- kidney sample: negative control

Supplementary Figure 1

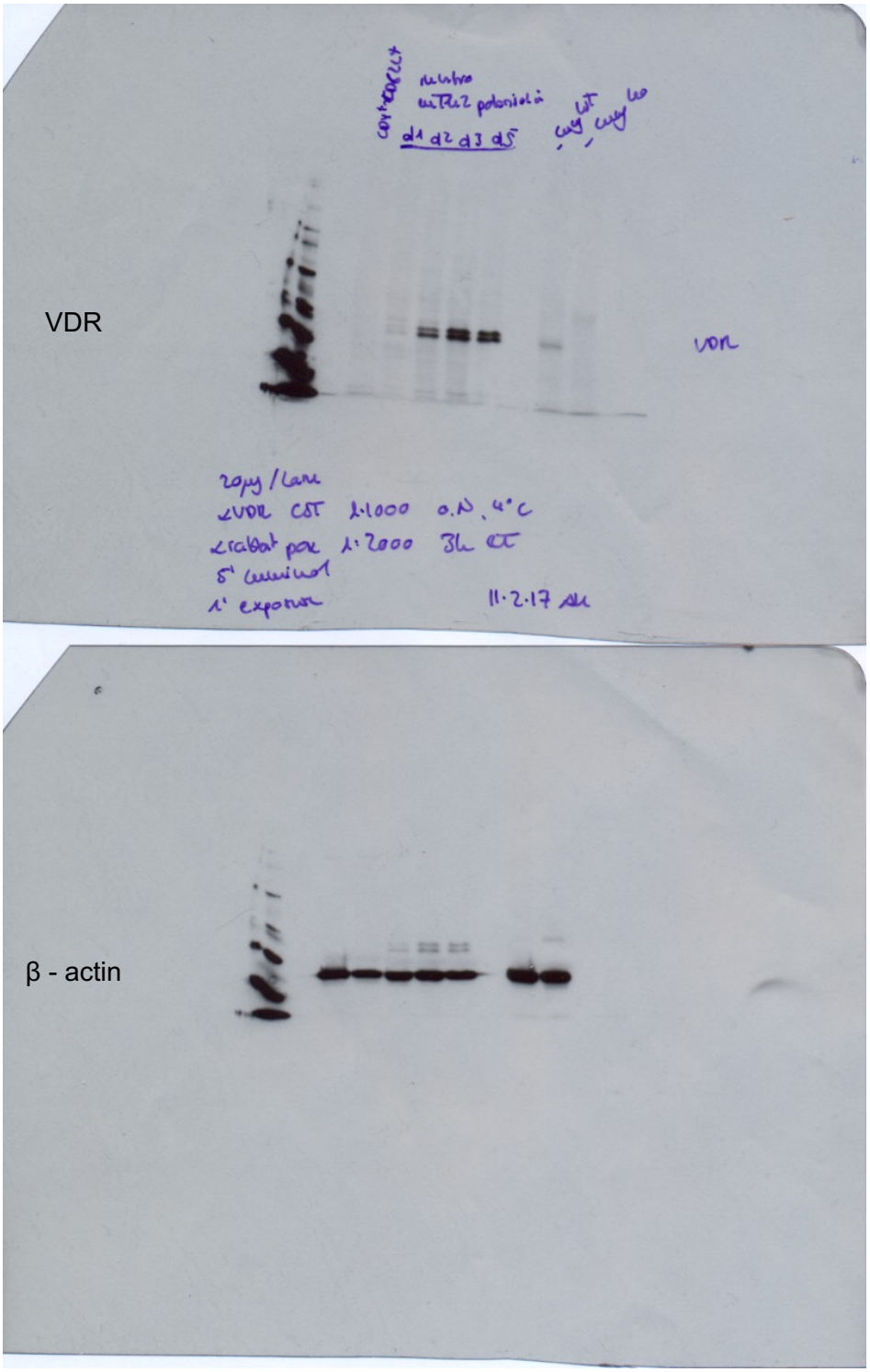

Loading order:
1- marker
2- empty
3- CD4+ CD62L+CD44- naïve T cells fresh
4- in vitro differentiating Th2 day 1
5- in vitro differentiating Th2 day 2
6- in vitro differentiating Th2 day 3
7- in vitro differentiating Th2 day 5
8- empty
9- WT lung sample: positive control
10- VDR-/- lung sample: negative control

Supplementary Figure 2